Electronic Supplementary Material (ESI) for Physical Chemistry Chemical Physics.

Spin-state energetics of metallocenes: How do best wave function and density functional results compare with the experimental data?

Electronic Supplementary Information (ESI)

Gabriela Drabik, Janusz Szklarzewicz, and Mariusz Radoń *

* Corresponding author
e-mail: mradon@chemia.uj.edu.pl

Table of contents

1. Full computational details

1.1 DFT calculations

Single-point calculations with 30 functionals were performed either using Turbomole (TPSS, TPSSh, PBE, PBE0, LH14t-calPBE, B2PLYP), ADF (S12g, S12h, SSB-D, MVS, MVSh) or Gaussian (M06L, M06, MN15, MN15L, M11, M11L, PW6B95, B3LYP, B3LYP*, BLYP, CAM-B3LYP, B97D, wB97XD, LCwPBE, LC-BLYP, BR, OLYP, O3LYP, OPBE). References to all functionals can be found in Section 10 of this document.

The Turbomole and Gaussian calculations employed the GTO basis set def2-QZVPP (metal, C) / def2-TZVPP (H) [S1-S3]. For ADF calculations we employed the Slater basis set ET-pVQZ (Mn, Fe, Co, C) / TZ2P (H) [S4]. For $RuCp_2$ the basis set was changed to ZORA-TZ4P (Ru, C) / ZORA-TZ2P (H), and the ZORA relativistic Hamiltonian was used as implemented in ADF [58]. The GTO (def2) basis set used for Ru in Gaussian and Turbomole calculations includes a relativistic pseudopotential [S1-S3]. For 3d-electron complexes, the relativistic correction was estimated at the second-order DKH level from separate B3LYP/cc-pVTZ(-DK) calculations performed with Gaussian (Tables S23-S25) and additively included (see Tables S26-S28); the same approach was used in ref 13.

The integration grid was “m5” in Turbomole, “UltraFine” in Gaussian, and “BeckeGrid (Quality VeryGood, RadialGridBoost 5)” in ADF. For hybrid functionals in ADF the “RIHartreeFock (Quality VeryGood)” option was used. The MP2 energy contribution to the B2PLYP functional was calculated with the RI approximation by correlating all electrons. The LH14t-calPBE functional was used within the RI-DFT approximation (as it is implemented in Turbomole).

1.2 WFT calculations

Table S1 defines the basis sets cT(D)-DK, cT(D)-NR, cT(D)-PP, used in this work along with the corresponding auxiliary basis sets for the F12 calculations (the auxiliary basis sets are identical as in ref 13). All F12 energies reported below includes the CABS singles correction. Total energies from all calculation can be found below in Section 5 (coupled cluster) and Section 7 (multireference).

1.3 Vibronic simulations

For the TI (time-independent) calculations we set MAXINT to 10^9, C1MAX to 50, C2MAX to 40, and decreased both thresholds $\varepsilon_{1,2}$ to 10^{-12}. With such settings, the recovered fraction of FC spectrum was 87% to 99%, and we were able to reach a good agreement between the TI and TD results, as shown below in Table S22 and Figures S3-S5.

Table S1. Basis sets cT(D)-DK, cT(D)-NR, cT(D)-PP, and auxiliary basis sets for F12 calculations.

	metal	C	H
cT(D)-DK	cc-pwCVTZ-DK [a]	cc-pVTZ-DK [b]	cc-pVDZ-DK [b]
cT(D)-NR	cc-pwCVTZ [a]	cc-pVTZ [c]	cc-pVDZ [c]
cT(D)-PP	cc-pwCVTZ-PP [d]	cc-pVTZ	cc-pVDZ
cT(D)-NR,df_basis [e]	aug-cc-pVTZ/mp2fit [f]	aug-cc-pVTZ/mp2fit [g]	aug-cc-pVDZ/mp2fit [g]
cT(D)-NR,df_basis_exch [h]	def2-TZVPP/jkfit [i]	aug-cc-pVTZ/jkfit [j]	aug-cc-pVDZ/jkfit [j]
cT(D)-NR,ri_basis [k]	def2-TZVPP/jkfit [h]	aug-cc-pVTZ/optri [l]	aug-cc-pVDZ/optri [l]
cT(D)-PP,df_basis [e]	aug-cc-pVTZ-PP/mp2fit [m]	aug-cc-pVTZ/mp2fit [g]	aug-cc-pVDZ/mp2fit [g]
cT(D)-PP,df_basis_exch [h]	def2-TZVPP/jkfit [i]	aug-cc-pVTZ/jkfit [j]	aug-cc-pVDZ/jkfit [j]
cT(D)-PP,ri_basis [k]	def2-TZVPP/jkfit [h]	aug-cc-pVTZ/optri [l]	aug-cc-pVDZ/optri [l]

[a] ref S5; [b] ref S8; [c] ref S7; [d] ref S6; [e] density fitting basis set; [f] ref S9; [g] ref S10; [h] density fitting basis set for the exchange and Fock operators; [i] ref S11; [j] ref S12; [k] basis set for RI; [l] ref S13, [m] ref S14.

2. Geometries

Complete dataset of geometry optimization and frequencies is also available in the ioChem-BD repository [Álvarez-Moreno et al., *J. Chem. Inf. Model.*, **2015**, 55, 95-103] under the following link: https://doi.org/10.19061/iochem-bd-7-4

Table S2. Cartesian coordinates for $MnCp_2$, doublet state optimized at PBE0/def2-TZVP level (eclipsed conformation distorted to C_{2v})

Mn	0.0000000	0.0000000	0.0043847
C	0.0000000	-1.8152137	1.1975619
H	0.0000000	-1.8322748	2.2777778
C	-1.1441924	-1.7680208	0.3729264
C	-0.7127594	-1.6943179	-0.9781097
C	0.7127594	-1.6943179	-0.9781097
C	1.1441924	-1.7680208	0.3729264
C	0.0000000	1.8152137	1.1975619
C	1.1441924	1.7680208	0.3729264
C	0.7127594	1.6943179	-0.9781097
C	-0.7127594	1.6943179	-0.9781097
C	-1.1441924	1.7680208	0.3729264
H	-2.1687608	-1.7665285	0.7145861
H	-1.3513990	-1.6675495	-1.8481688
H	1.3513990	-1.6675495	-1.8481688
H	2.1687608	-1.7665285	0.7145861
H	0.0000000	1.8322748	2.2777778
H	2.1687608	1.7665285	0.7145861
H	1.3513990	1.6675495	-1.8481688
H	-1.3513990	1.6675495	-1.8481688
H	-2.1687608	1.7665285	0.7145861

Table S3. Cartesian coordinates in Angstrom for $MnCp_2$, doublet state optimized at BP86/def2-TZVP level (eclipsed conformation distorted to C_{2v})

Mn	0.0000000	0.0000000	0.0081912
C	0.0000000	-1.8244748	1.2062801
H	0.0000000	-1.8548493	2.2932584
C	-1.1536348	-1.7674145	0.3765074
C	-0.7202906	-1.6778875	-0.9871867
C	0.7202906	-1.6778875	-0.9871867
C	1.1536348	-1.7674145	0.3765074
C	0.0000000	1.8244748	1.2062801
C	1.1536348	1.7674145	0.3765074
C	0.7202906	1.6778875	-0.9871867
C	-0.7202906	1.6778875	-0.9871867
C	-1.1536348	1.7674145	0.3765074
H	-2.1845222	-1.7740911	0.7216315
H	-1.3637993	-1.6563219	-1.8627692
H	1.3637993	-1.6563219	-1.8627692
H	2.1845222	-1.7740911	0.7216315
H	0.0000000	1.8548493	2.2932584
H	2.1845222	1.7740911	0.7216315
H	1.3637993	1.6563219	-1.8627692
H	-1.3637993	1.6563219	-1.8627692
H	-2.1845222	1.7740911	0.7216315

Table S4. Cartesian coordinates in Angstrom for $MnCp_2$, sextet state optimized at PBE0/def2-TZVP level (eclipsed conformation, D_{5d})

Mn	-0.0000000	0.0000000	0.0000000
C	0.0000000	1.2037557	2.0620032
H	0.0000000	2.2843914	2.0764353
C	-0.7075498	0.9738588	-2.0620032
C	-1.1448397	0.3719810	2.0620032
C	-1.1448397	-0.3719810	-2.0620032
C	-0.7075498	-0.9738588	2.0620032
C	0.0000000	-1.2037557	-2.0620032
C	0.7075498	-0.9738588	2.0620032
C	1.1448397	-0.3719810	-2.0620032
C	1.1448397	0.3719810	2.0620032
C	0.7075498	0.9738588	-2.0620032
H	-1.3427316	1.8481115	-2.0764353
H	-2.1725853	0.7059158	2.0764353
H	-2.1725853	-0.7059158	-2.0764353
H	-1.3427316	-1.8481115	2.0764353
H	0.0000000	-2.2843914	-2.0764353
H	1.3427316	-1.8481115	2.0764353
H	2.1725853	-0.7059158	-2.0764353
H	2.1725853	0.7059158	2.0764353
H	1.3427316	1.8481115	-2.0764353

Table S5. Cartesian coordinates in Angstrom for $MnCp_2$, sextet state at optimized BP86/def2-TZVP level (eclipsed conformation distorted to C_2)

Mn	-0.0000000	0.0000000	0.4538171
C	1.0531570	-1.9311495	-0.6242995
H	1.9993888	-1.8526654	-1.1536095
C	0.8958395	-2.1121087	0.7804746
C	-0.5074308	-2.1544161	1.0630707
C	-1.2047687	-2.0002504	-0.1731306
C	-0.2408129	-1.8614228	-1.2078113
C	1.2047687	2.0002504	-0.1731306
C	0.2408129	1.8614228	-1.2078113
C	-1.0531570	1.9311495	-0.6242995
C	-0.8958395	2.1121087	0.7804746
C	0.5074308	2.1544161	1.0630707
H	1.6965512	-2.2376405	1.5057582
H	-0.9580568	-2.3288087	2.0374830
H	-2.2848191	-1.9934222	-0.2976192
H	-0.4568592	-1.7062615	-2.2617046
H	2.2848191	1.9934222	-0.2976192
H	0.4568592	1.7062615	-2.2617046
H	-1.9993888	1.8526654	-1.1536095
H	-1.6965512	2.2376405	1.5057582
H	0.9580568	2.3288087	2.0374830

Table S6. Cartesian coordinates in Angstrom for $FeCp_2$, singlet ground state optimized at BP86/ def2-TZVP level (eclipsed conformation, D_{5h}).

Fe	0.0000000	0.0000000	0.0000000
C	-1.2198992	0.0000000	1.6501014
C	-0.3769696	-1.1601931	1.6501014
C	0.9869192	-0.7170388	1.6501014
C	0.9869192	0.7170388	1.6501014
C	-0.3769696	1.1601931	1.6501014
H	-2.3063625	0.0000000	1.6353877
H	-0.7127052	-2.1934811	1.6353877
H	1.8658864	-1.3556459	1.6353877
H	1.8658864	1.3556459	1.6353877
H	-0.7127052	2.1934811	1.6353877
C	-1.2198992	0.0000000	-1.6501014
C	-0.3769696	-1.1601931	-1.6501014
C	0.9869192	-0.7170388	-1.6501014
C	0.9869192	0.7170388	-1.6501014
C	-0.3769696	1.1601931	-1.6501014
H	-2.3063625	0.0000000	-1.6353877
H	-0.7127052	-2.1934811	-1.6353877
H	1.8658864	-1.3556459	-1.6353877
H	1.8658864	1.3556459	-1.6353877
H	-0.7127052	2.1934811	-1.6353877

Table S7. Cartesian coordinates in Angstrom for $FeCp_2$, singlet ground state optimized at PBE0/ def2-TZVP level (eclipsed conformation, D_{5h}).

Fe	0.0000000	0.0000000	-0.0000000
C	-1.2081981	0.0000000	1.6516020
C	-0.3733538	-1.1490647	1.6516020
C	0.9774528	-0.7101610	1.6516020
C	0.9774528	0.7101610	1.6516020
C	-0.3733538	1.1490647	1.6516020
H	-2.2873722	0.0000000	1.6281017
H	-0.7068369	-2.1754202	1.6281017
H	1.8505230	-1.3444836	1.6281017
H	1.8505230	1.3444836	1.6281017
H	-0.7068369	2.1754202	1.6281017
C	-1.2081981	0.0000000	-1.6516020
C	-0.3733538	-1.1490647	-1.6516020
C	0.9774528	-0.7101610	-1.6516020
C	0.9774528	0.7101610	-1.6516020
C	-0.3733538	1.1490647	-1.6516020
H	-2.2873722	0.0000000	-1.6281017
H	-0.7068369	-2.1754202	-1.6281017
H	1.8505230	-1.3444836	-1.6281017
H	1.8505230	1.3444836	-1.6281017
H	-0.7068369	2.1754202	-1.6281017

Table S8. Cartesian coordinates in Angstrom for $FeCp_2$, triplet excited state (T_1) optimized at BP86/ def2-TZVP level (eclipsed conformation distorted to C_{2v}).

Fe	0.0000000	0.0000000	0.0508218
C	-1.8994594	0.0000000	-1.2196099
C	-1.7982169	-1.1445806	-0.3842855
C	-1.7881323	-0.7104224	0.9917145
C	-1.7881323	0.7104224	0.9917145
C	-1.7982169	1.1445806	-0.3842855
H	-1.9012479	0.0000000	-2.3063672
H	-1.7994916	-2.1791636	-0.7182122
H	-1.7849683	-1.3617603	1.8610662
H	-1.7849683	1.3617603	1.8610662
H	-1.7994916	2.1791636	-0.7182122
C	1.8994594	0.0000000	-1.2196099
C	1.7982169	-1.1445806	-0.3842855
C	1.7881323	-0.7104224	0.9917145
C	1.7881323	0.7104224	0.9917145
C	1.7982169	1.1445806	-0.3842855
H	1.9012479	0.0000000	-2.3063672
H	1.7994916	-2.1791636	-0.7182122
H	1.7849683	-1.3617603	1.8610662
H	1.7849683	1.3617603	1.8610662
H	1.7994916	2.1791636	-0.7182122

Table S9. Cartesian coordinates in Angstrom for $FeCp_2$, triplet excited state (T_1) optimized at PBE0/ def2-TZVP level (eclipsed conformation distorted to C_{2v}).

Fe	0.0000000	0.0000000	0.0321592
C	-1.8948801	0.0000000	-1.2095604
C	-1.8116043	-1.1355480	-0.3793778
C	-1.8074633	-0.7033090	0.9832655
C	-1.8074633	0.7033090	0.9832655
C	-1.8116043	1.1355480	-0.3793778
H	-1.8961098	0.0000000	-2.2894992
H	-1.8070380	-2.1636580	-0.7111738
H	-1.7973307	-1.3484443	1.8487761
H	-1.7973307	1.3484443	1.8487761
H	-1.8070380	2.1636580	-0.7111738
C	1.8948801	0.0000000	-1.2095604
C	1.8116043	-1.1355480	-0.3793778
C	1.8074633	-0.7033090	0.9832655
C	1.8074633	0.7033090	0.9832655
C	1.8116043	1.1355480	-0.3793778
H	1.8961098	0.0000000	-2.2894992
H	1.8070380	-2.1636580	-0.7111738
H	1.7973307	-1.3484443	1.8487761
H	1.7973307	1.3484443	1.8487761
H	1.8070380	2.1636580	-0.7111738

Table S10. Cartesian coordinates in Angstrom for $[CoCp_2]+$, singlet ground state optimized at BP86/def2-TZVP level (eclipsed conformation, D_{5h})

Co	0.0000000	-0.0000000	0.0000000
C	1.2188782	0.0000000	1.6545782
H	2.3051570	0.0000000	1.6353329
C	0.3766541	1.1592221	1.6545782
C	-0.9860932	0.7164386	1.6545782
C	-0.9860932	-0.7164386	1.6545782
C	0.3766541	-1.1592221	1.6545782
C	1.2188782	0.0000000	-1.6545782
C	0.3766541	-1.1592221	-1.6545782
C	-0.9860932	-0.7164386	-1.6545782
C	-0.9860932	0.7164386	-1.6545782
C	0.3766541	1.1592221	-1.6545782
H	0.7123327	2.1923346	1.6353329
H	-1.8649112	1.3549373	1.6353329
H	-1.8649112	-1.3549373	1.6353329
H	0.7123327	-2.1923346	1.6353329
H	2.3051570	0.0000000	-1.6353329
H	0.7123327	-2.1923346	-1.6353329
H	-1.8649112	-1.3549373	-1.6353329
H	-1.8649112	1.3549373	-1.6353329
H	0.7123327	2.1923346	-1.6353329

Table S11. Cartesian coordinates in Angstrom for $[CoCp_2]+$, singlet ground state optimized at PBE0/def2-TZVP level (eclipsed conformation, D_{5h})

Co	-0.0000000	-0.0000000	0.0000000
C	1.2079519	0.0000000	1.6426949
H	2.2872673	0.0000000	1.6133697
C	0.3732777	1.1488305	1.6426949
C	-0.9772536	0.7100163	1.6426949
C	-0.9772536	-0.7100163	1.6426949
C	0.3732777	-1.1488305	1.6426949
C	1.2079519	0.0000000	-1.6426949
C	0.3732777	-1.1488305	-1.6426949
C	-0.9772536	-0.7100163	-1.6426949
C	-0.9772536	0.7100163	-1.6426949
C	0.3732777	1.1488305	-1.6426949
H	0.7068045	2.1753205	1.6133697
H	-1.8504381	1.3444220	1.6133697
H	-1.8504381	-1.3444220	1.6133697
H	0.7068045	-2.1753205	1.6133697
H	2.2872673	0.0000000	-1.6133697
H	0.7068045	-2.1753205	-1.6133697
H	-1.8504381	-1.3444220	-1.6133697
H	-1.8504381	1.3444220	-1.6133697
H	0.7068045	2.1753205	-1.6133697

Table S12. Cartesian coordinates in Angstrom for $[CoCp_2]^+$, triplet excited state (T_1) optimized at BP86/def2-TZVP level (eclipsed conformation distorted to C_{2v}).

Co	0.0000000	0.0000000	0.1662965
C	-1.9680294	0.0000000	1.2009853
H	-2.0765993	0.0000000	2.2829010
C	-1.8006396	1.1485240	0.3756728
C	-1.6872851	0.7053479	-0.9989880
C	-1.6872851	-0.7053479	-0.9989880
C	-1.8006396	-1.1485240	0.3756728
C	1.9680294	0.0000000	1.2009853
C	1.8006396	-1.1485240	0.3756728
C	1.6872851	-0.7053479	-0.9989880
C	1.6872851	0.7053479	-0.9989880
C	1.8006396	1.1485240	0.3756728
H	-1.8333578	2.1837731	0.7053009
H	-1.5978441	1.3543773	-1.8655029
H	-1.5978441	-1.3543773	-1.8655029
H	-1.8333578	-2.1837731	0.7053009
H	2.0765993	0.0000000	2.2829010
H	1.8333578	-2.1837731	0.7053009
H	1.5978441	-1.3543773	-1.8655029
H	1.5978441	1.3543773	-1.8655029
H	1.8333578	2.1837731	0.7053009

Table S13. Cartesian coordinates in Angstrom for $[CoCp_2]^+$, triplet excited state (T_1) optimized at PBE0/def2-TZVP level (eclipsed conformation distorted to C_{2v}).

Co	0.0000000	0.0000000	-0.0004515
C	-1.8653634	0.0000000	1.2140988
H	-1.8853532	0.0000000	2.2938466
C	-1.7887528	1.1361147	0.3818028
C	-1.7779960	0.6986649	-0.9909284
C	-1.7779960	-0.6986649	-0.9909284
C	-1.7887528	-1.1361147	0.3818028
C	1.8653634	0.0000000	1.2140988
C	1.7887528	-1.1361147	0.3818028
C	1.7779960	-0.6986649	-0.9909284
C	1.7779960	0.6986649	-0.9909284
C	1.7887528	1.1361147	0.3818028
H	-1.7856965	2.1655683	0.7108488
H	-1.7608016	1.3452849	-1.8555830
H	-1.7608016	-1.3452849	-1.8555830
H	-1.7856965	-2.1655683	0.7108488
H	1.8853532	0.0000000	2.2938466
H	1.7856965	-2.1655683	0.7108488
H	1.7608016	-1.3452849	-1.8555830
H	1.7608016	1.3452849	-1.8555830
H	1.7856965	2.1655683	0.7108488

Table S14. Cartesian coordinates in Angstrom for $RuCp_2$, singlet ground state optimized at BP86/ def2-TZVP level (eclipsed conformation, D_{5h})

Ru	0.0000000	0.0000000	0.0000000
C	1.2218861	0.0000000	1.8159510
H	2.3080643	0.0000000	1.8282169
C	0.3775836	1.1620827	1.8159510
C	-0.9885266	0.7182066	1.8159510
C	-0.9885266	-0.7182066	1.8159510
C	0.3775836	-1.1620827	1.8159510
C	1.2218861	0.0000000	-1.8159510
C	0.3775836	-1.1620827	-1.8159510
C	-0.9885266	-0.7182066	-1.8159510
C	-0.9885266	0.7182066	-1.8159510
C	0.3775836	1.1620827	-1.8159510
H	0.7132311	2.1950996	1.8282169
H	-1.8672633	1.3566462	1.8282169
H	-1.8672633	-1.3566462	1.8282169
H	0.7132311	-2.1950996	1.8282169
H	2.3080643	0.0000000	-1.8282169
H	0.7132311	-2.1950996	-1.8282169
H	-1.8672633	-1.3566462	-1.8282169
H	-1.8672633	1.3566462	-1.8282169
H	0.7132311	2.1950996	-1.8282169

Table S15. Cartesian coordinates in Angstrom for $RuCp_2$, singlet ground state optimized at PBE0/ def2-TZVP level (eclipsed conformation, D_{5h})

Ru	-0.0000000	-0.0000000	0.0000000
C	1.2118803	0.0000000	1.7990841
H	2.2912112	0.0000000	1.8074587
C	0.3744916	1.1525666	1.7990841
C	-0.9804317	0.7123254	1.7990841
C	-0.9804317	-0.7123254	1.7990841
C	0.3744916	-1.1525666	1.7990841
C	1.2118803	0.0000000	-1.7990841
C	0.3744916	-1.1525666	-1.7990841
C	-0.9804317	-0.7123254	-1.7990841
C	-0.9804317	0.7123254	-1.7990841
C	0.3744916	1.1525666	-1.7990841
H	0.7080232	2.1790714	1.8074587
H	-1.8536288	1.3467402	1.8074587
H	-1.8536288	-1.3467402	1.8074587
H	0.7080232	-2.1790714	1.8074587
H	2.2912112	0.0000000	-1.8074587
H	0.7080232	-2.1790714	-1.8074587
H	-1.8536288	-1.3467402	-1.8074587
H	-1.8536288	1.3467402	-1.8074587
H	0.7080232	2.1790714	-1.8074587

Table S16. Cartesian coordinates for $RuCp_2$, lowest triplet excited state T_1 optimized at BP86/def2-TZVP level (distorted to C_2).

Ru	0.0000000	0.0000000	-0.4202308
C	-1.7928378	0.1012715	1.2302439
H	-1.6149528	0.2549532	2.2902983
C	-1.8754994	1.1280599	0.2277546
C	-2.0930581	0.5056469	-1.0437380
C	-1.9978345	-0.9155243	-0.8576720
C	-1.7628860	-1.1439043	0.5435679
C	1.7928378	-0.1012715	1.2302439
C	1.8754994	-1.1280599	0.2277546
C	2.0930581	-0.5056469	-1.0437380
C	1.9978345	0.9155243	-0.8576720
C	1.7628860	1.1439043	0.5435679
H	-1.8911111	2.1988166	0.4113600
H	-2.2723786	1.0251631	-1.9812230
H	-2.1368894	-1.6830997	-1.6129984
H	-1.6462833	-2.1223098	1.0025222
H	1.6149528	-0.2549532	2.2902983
H	1.8911111	-2.1988166	0.4113600
H	2.2723786	-1.0251631	-1.9812230
H	2.1368894	1.6830997	-1.6129984
H	1.6462833	2.1223098	1.0025222

Table S17. Cartesian coordinates for $RuCp_2$, lowest triplet excited state T_1 optimized at BP86/def2-TZVP level (eclipsed distorted to C_{2v} with an imaginary frequency; the "BP86*" structure).

Ru	0.0000000	0.0000000	-0.4114325
C	-1.7943046	0.0000000	1.2415824
H	-1.6126724	0.0000000	2.3120160
C	-1.8204104	1.1476721	0.3890183
C	-2.0532921	0.7181613	-0.9606003
C	-2.0532921	-0.7181613	-0.9606003
C	-1.8204104	-1.1476721	0.3890183
C	1.7943046	0.0000000	1.2415824
C	1.8204104	-1.1476721	0.3890183
C	2.0532921	-0.7181613	-0.9606003
C	2.0532921	0.7181613	-0.9606003
C	1.8204104	1.1476721	0.3890183
H	-1.7681753	2.1837592	0.7127595
H	-2.2151842	1.3688863	-1.8151185
H	-2.2151842	-1.3688863	-1.8151185
H	-1.7681753	-2.1837592	0.7127595
H	1.6126724	0.0000000	2.3120160
H	1.7681753	-2.1837592	0.7127595
H	2.2151842	-1.3688863	-1.8151185
H	2.2151842	1.3688863	-1.8151185
H	1.7681753	2.1837592	0.7127595

Table S18. Cartesian coordinates for $RuCp_2$, lowest triplet excited state T_1 optimized at PBE0/def2-TZVP level (eclipsed conformation distorted to C_{2v}).

Ru	0.0000000	0.0000000	-0.1264330
C	-2.0250281	0.0000000	1.2190229
H	-2.0066822	0.0000000	2.2986369
C	-1.9289300	1.1359722	0.3835563
C	-1.9646372	0.7075942	-0.9804475
C	-1.9646372	-0.7075942	-0.9804475
C	-1.9289300	-1.1359722	0.3835563
C	2.0250281	0.0000000	1.2190229
C	1.9289300	-1.1359722	0.3835563
C	1.9646372	-0.7075942	-0.9804475
C	1.9646372	0.7075942	-0.9804475
C	1.9289300	1.1359722	0.3835563
H	-1.9300578	2.1649020	0.7123345
H	-2.0044180	1.3556059	-1.8426649
H	-2.0044180	-1.3556059	-1.8426649
H	-1.9300578	-2.1649020	0.7123345
H	2.0066822	0.0000000	2.2986369
H	1.9300578	-2.1649020	0.7123345
H	2.0044180	-1.3556059	-1.8426649
H	2.0044180	1.3556059	-1.8426649
H	1.9300578	2.1649020	0.7123345

Table S19. Cartesian coordinates for $RuCp_2$, lowest triplet excited state T_1 optimized at UHF-CCSD(T)/cT(D)-PP level (eclipsed conformation distorted to C_{2v}).

Ru	0.000000	0.000000	0.000000
C	2.046376	0.000000	-1.300217
C	-2.046376	0.000000	-1.300217
C	1.939563	-1.142962	-0.462880
C	1.939563	1.142962	-0.462880
C	-1.939563	1.142962	-0.462880
C	-1.939563	-1.142962	-0.462880
C	1.954748	-0.710255	0.910350
C	1.954748	0.710255	0.910350
C	-1.954748	0.710255	0.910350
C	-1.954748	-0.710255	0.910350
H	2.046445	0.000000	-2.384316
H	-2.046445	0.000000	-2.384316
H	1.950510	-2.175687	-0.792880
H	1.950510	2.175687	-0.792880
H	-1.950510	2.175687	-0.792880
H	-1.950510	-2.175687	-0.792880
H	1.976990	-1.360426	1.776610
H	1.976990	1.360426	1.776610
H	-1.976990	1.360426	1.776610
H	-1.976990	-1.360426	1.776610

Table S20. Z-matrix used to optimize geometry of T_1 state for $RuCp_2$ at the CCSD(T) level with the CFour program. Final values of the optimized parameters (*) are listed.

```
Ru
X 1 RRX1
X 1 RRX* 2 A90
X 1 RRX* 2 A90 3 D180
C 3 RXC1* 1 ARXC* 2 D180
C 4 RXC1* 1 ARXC* 2 D180
C 3 RXC2* 5 A72A* 1 D90
C 3 RXC2* 5 A72A* 7 D180
C 4 RXC2* 6 A72A* 1 D90
C 4 RXC2* 6 A72A* 9 D180
X 3 RXX 1 ARXX* 2 D0
X 4 RXX 1 ARXX* 2 D0
C 3 RXC3* 7 A72B* 11 D0
C 3 RXC3* 8 A72B* 11 D0
C 4 RXC3* 9 A72B* 12 D0
C 4 RXC3* 10 A72B* 12 D0
H 5 RCH1* 1 ARCH1* 2 D180
H 6 RCH1* 1 ARCH1* 2 D180
X 1 RRX1 2 A108A* 3 D90
X 1 RRX1 2 A108A* 19 D180
H 7 RCH2* 1 ARCH2* 19 D0
H 8 RCH2* 1 ARCH2* 20 D0
H 9 RCH2* 1 ARCH2* 20 D0
H 10 RCH2* 1 ARCH2* 19 D0
X 1 RRX1 2 A36A* 3 D90
X 1 RRX1 2 A36A* 25 D180
H 13 RCH3* 1 ARCH3* 25 D0
H 14 RCH3* 1 ARCH3* 26 D0
H 15 RCH3* 1 ARCH3* 26 D0
H 16 RCH3* 1 ARCH3* 25 D0

RRX1 =        1.000000000000000
RRX  =        1.880516883692004
A90  =       90.000000000000000
D180 =      180.000000000000000
RXC1 =        1.310753390581075
ARXC =       97.269530276269620
RXC2 =        1.234546567766365
A72A =       67.791545890431593
D90  =       90.000000000000014
RXX  =        1.000000000000000
ARXX =       91.794773138777956
D0   =        0.000000000000000
RXC3 =        1.157025981898399
A72B =       73.955197780349110
RCH1 =        1.084098269805931
ARCH1=      122.434554635556111
A108A=      107.692974205741422
RCH2 =        1.084223520403107
ARCH2=      122.921461864473528
A36A =       36.876869293214803
RCH3 =        1.083338853378630
ARCH3=      121.740158175388146
```

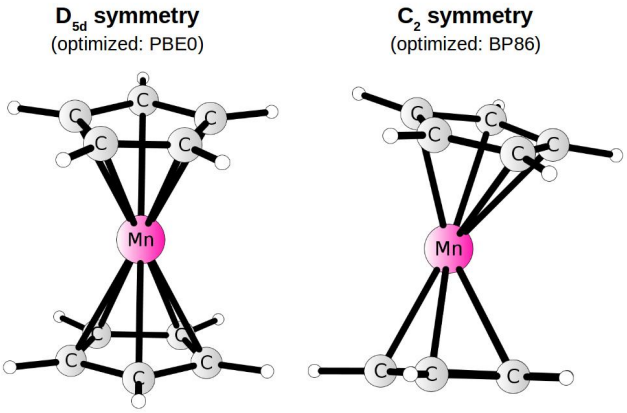

Figure S1. Structures of ^{6}[$MnCp_2$] optimized with PBE0 (*left*) and BP86 (*right*) functionals.

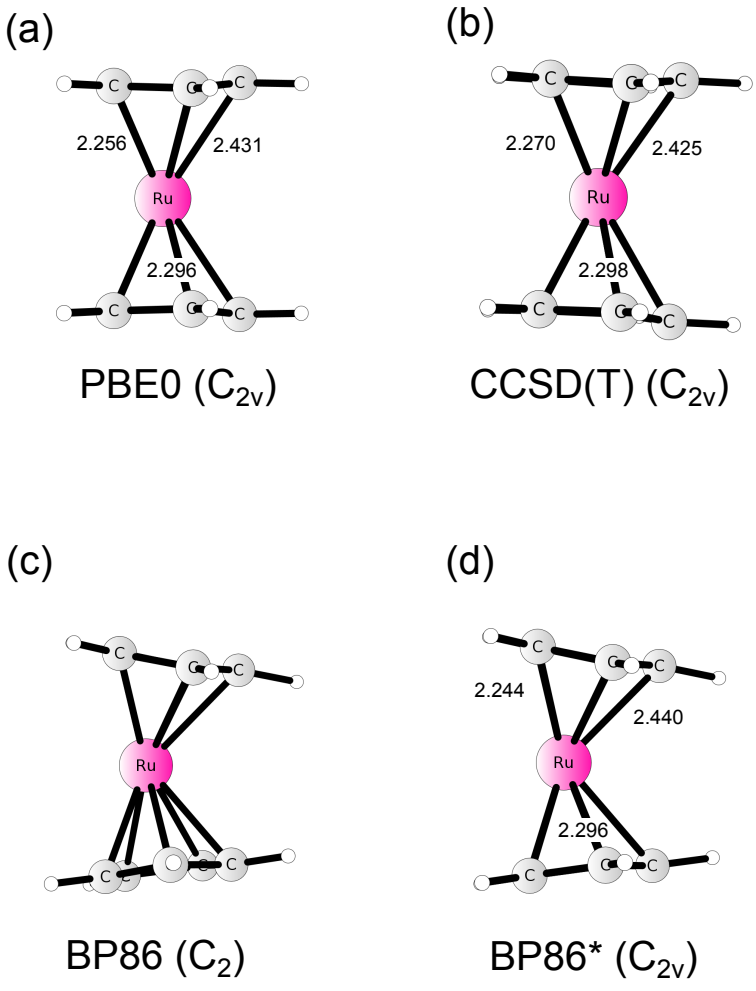

Figure S2. Structures of ^{3}[$RuCp_2$] (T_1 state) optimized at various theory levels: (a) PBE0/def2-TZVP; (b) UHF-CCSD(T)/cT(D)-PP; (c) BP86/def2-TZVP. Panel (d) called "BP86*" the same as theory level as (c), but with the geometry constrained to C_{2v} symmetry, so that imaginary frequency of *i*7 cm^{-1} appears, but the energy is higher than the fully optimized one (C_2 symmetry) only by 0.006 kcal/mol. Numbers annotated on structures in (a), (b) and (d) are the Ru-C bond lengths in Angstrom.

3. Vibrational corrections

Table S21. Enthalpy correction for doublet ⇌ sextet SCO equilibrium of $MnCp_2$.

	$H - E_e$ (kJ/mol)		$\Delta H - \Delta E_e$ (eV)
	(S=1/2)	(S=5/2)	
PBE0, T=212K [a]	458.38	452.87	-0.06
PBE0, T=298 K	470.26	465.67	-0.05
BP86, T=212 K [a]	441.60	438.27	-0.03

[a] T=212 K is the T(1/2) temperature calculated as (experimental) $\Delta H/\Delta S$ ratio.

Table S22. Vibronic corrections to vertical energies determined with FCclasses v.3 using PBE0 or BP86/def2-TZVP geometries and harmonic frequencies. All energy values in eV.

	$Ru(Cp)_2$, $S_0 \rightarrow T_1$			$Ru(Cp)_2$, $T_1 \rightarrow S_0$	$Fe(Cp)_2$, $S_0 \rightarrow T_1$		$[Co(Cp)_2]^+$, $S_0 \rightarrow T_1$	
	PBE0	BP86*	BP86	PBE0	PBE0	BP86	PBE0	BP86
ΔE_{ad} [a]	2.6215	2.6275	2.6273	2.6215	0.8194	1.5109	1.2752	1.9559
ΔE_{vert} [b]	3.4530	3.4390	3.4388	1.7315	1.5503	2.1585	1.9273	2.5448
ΔZPE [c]	-0.1132	-0.1054	-0.1066	-0.1132	-0.1030	-0.0966	-0.1331	-0.1020
ΔE_{vert}^{harm} [d]	3.3622	3.8186	3.9786	1.4704	1.4124	2.0640	1.8096	2.5543
ΔE_{max}^{harm} (0K), TD [e]	3.2525	3.7075	3.845	1.5100	1.3200	1.9600	1.6850	2.4450
ΔE_{max}^{harm} (0K), TI [e]	3.2450	na	na	1.5225	1.3200	1.9600	1.6850	2.4375
% FC spec. TI (0K) [f]	93.0	na	na	86.8	98.4	98.6	98.7	92.7
ΔE_{max}^{harm}, TD (300K) [e]	3.2550	3.7100	3.865	1.4450	1.3200	1.9575	1.6875	2.4425
δ^{harm} (0K) [g]	-0.1097	-0.1111	**-0.1336**	**0.0396**	-0.0924	**-0.1040**	-0.1246	**-0.1093**
δ^{harm} (300 K) [g]	-0.1072	-0.1086	-0.1136	-0.0254	-0.0924	-0.1065	-0.1221	-0.1118

[a] Adiabatic energy $E(T_1) - E(S_0)$ at the DFT level. [b] Vertical energy $E(T_1) - E(S_0)$ at the DFT level. [c] Zero-point energy difference $ZPE(T_1) - ZPE(S_0)$ at the DFT level. [d] Harmonic approximation of the vertical energy based on DFT geometries and frequencies. [e] Maximum of the spectrum simulated with FCclasses using TD or TI approach, at given temperature. [f] Percentage of Franck-Condon spectrum recovered using TI approach at temperature 0 K. [g] Vibronic correction to vertical energy (see main article); calculated as the difference between the maximum of the simulated spectrum and corresponding harmonic approximation of the vertical energy, $\delta^{harm} = \Delta E_{max}^{harm} - \Delta E_{vert}^{harm}$, at given temperature.
"BP86*" - For this BP86 optimization the geometry of T_1 state was constrained to C_{2v} symmetry instead of true C_2 symmetry (see main article); resulting imaginary frequency of $i6.75$ cm^{-1} was converted to +6.75 cm^{-1}.
"na" = not available because the calculations did not converge.

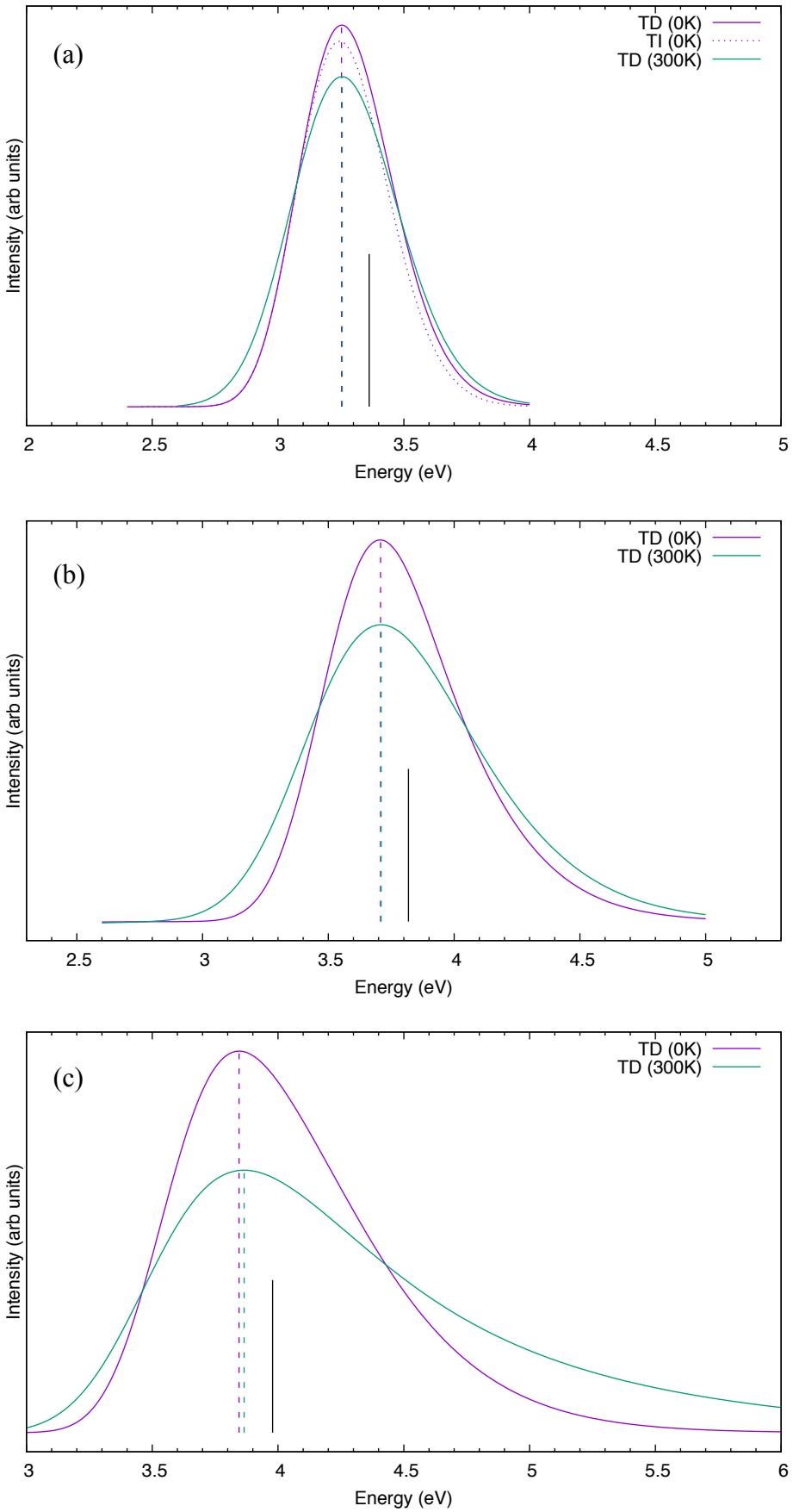

Figure S3. Vibrational progressions of $S_0 \rightarrow T_1$ band for $RuCp_2$ simulated from on (a) PBE0, (b) BP86*, and (c) BP86 data (adiab. energy, geometries and harmonic freq.). Black vertical line is harmonic vertical energy of each method. Acronym "BP86*" explained in prev. table.

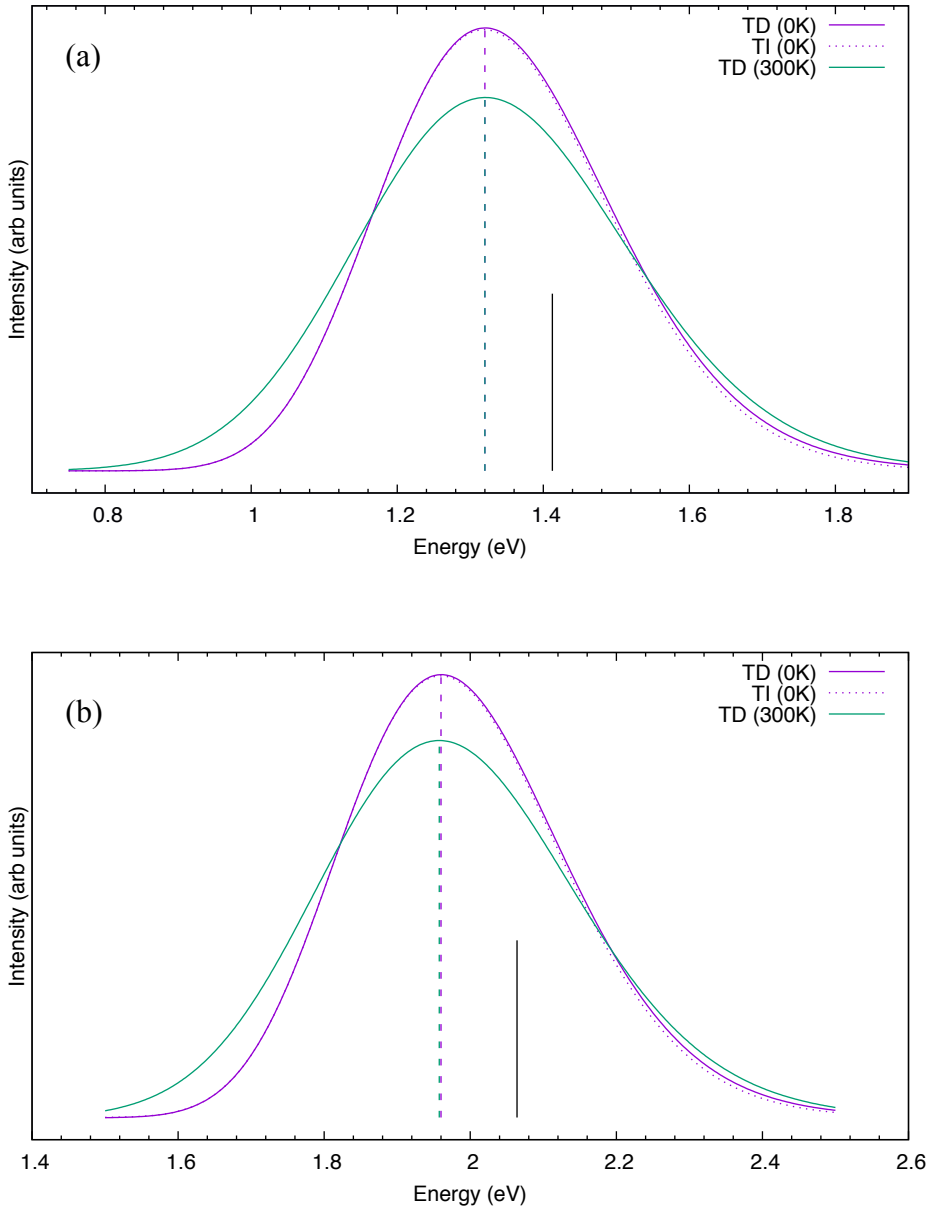

Figure S4. Vibrational progressions of $S_0 \rightarrow T_1$ band for $FeCp_2$ simulated from on (a) PBE0 and (b) BP86 data (adiabatic energy, geometries and harmonic frequencies). Black vertical line is harmonic vertical energy of each method.

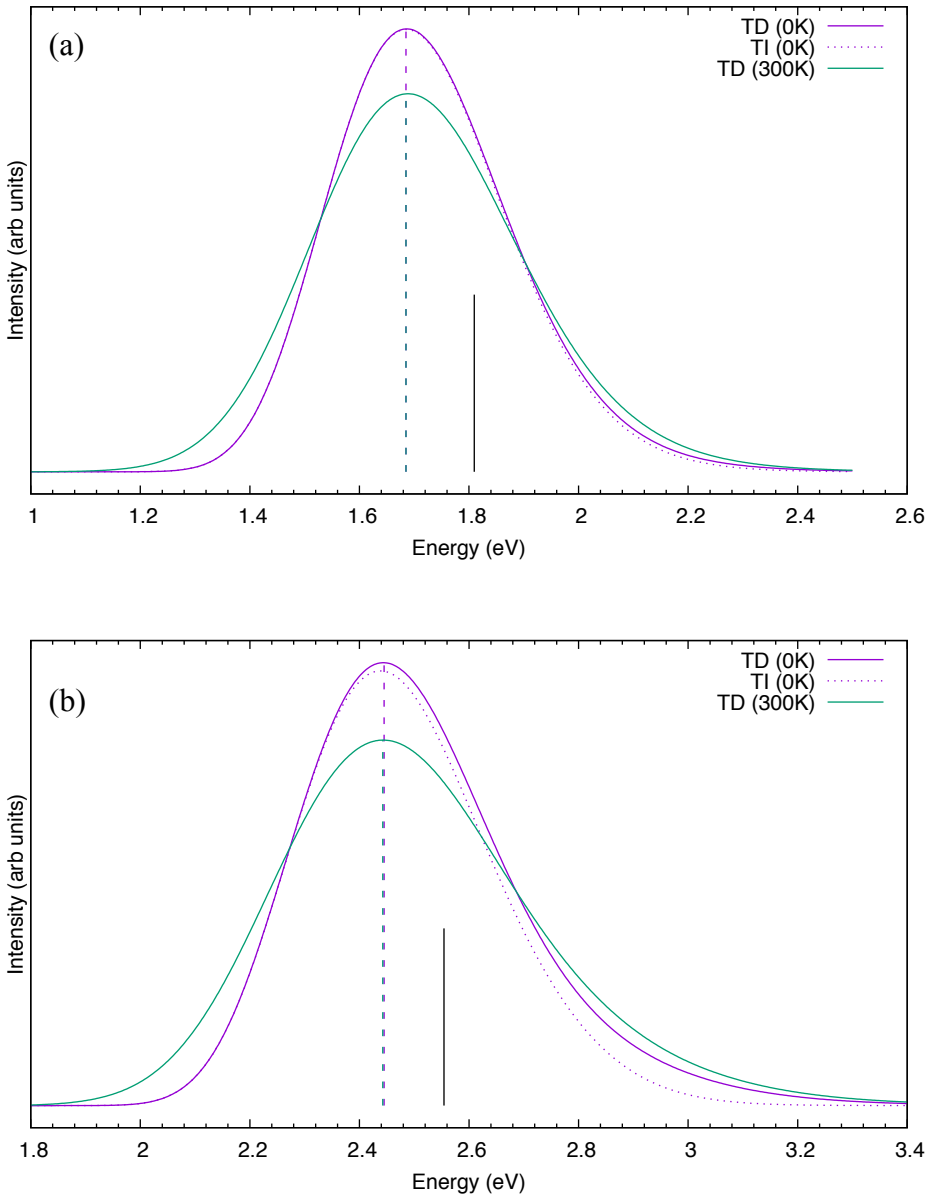

Figure S5. Vibrational progressions of $S_0 \rightarrow T_1$ band for $FeCp_2$ simulated from on (a) PBE0 and (b) BP86 data (adiabatic energy, geometries and harmonic frequencies). Black vertical line is harmonic vertical energy for each method.

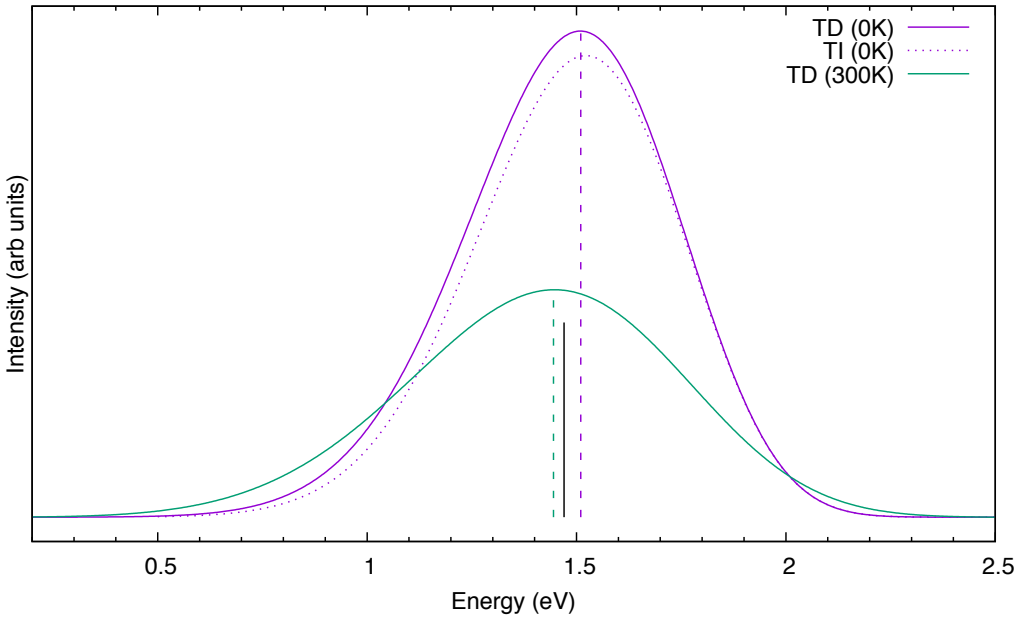

Figure S6. Vibrational progressions of $T_1 \rightarrow S_0$ band for $RuCp_2$ simulated from PBE0 adiabatic energy, geometries and harmonic frequencies. Black vertical line is harmonic vertical energy.

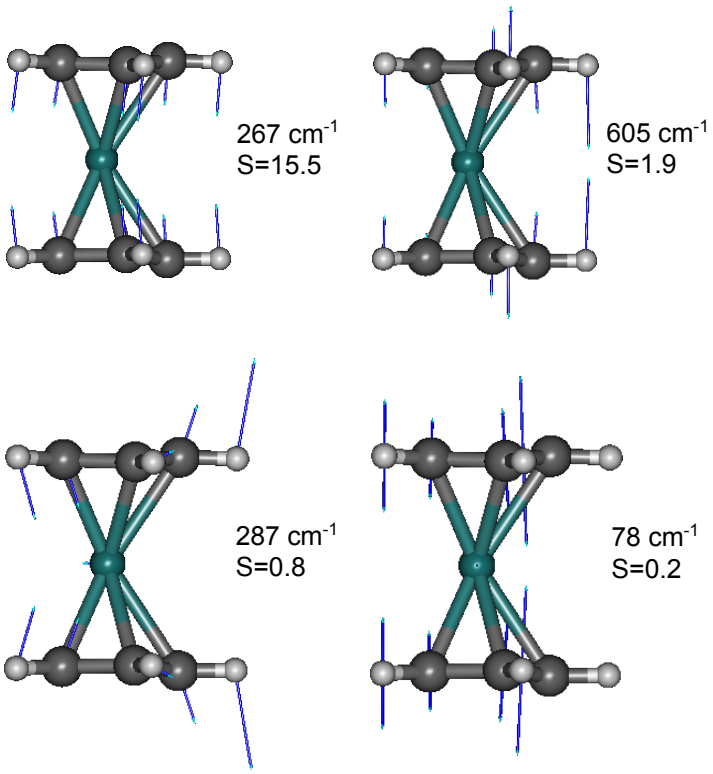

Figure S7. Four vibrational modes of the T_1 state of $RuCp_2$ most relevant for vibrational progression in the $S_0 \rightarrow T_1$ absorption band with indicated values of Huang-Rhys parameter *S*. Based on PBE0/ def2-TZVP geometries and frequencies. Compare with Figure 6, main article

4. Detailed DFT results

Table S23: Non-relativistic and DKH2-relativistic DFT:B3LYP results for [$MnCp_2$] doublet-sextet adiabatic energy to determine the relativistic correction.

	E (S=1/2) (a.u.)	$<S^2>$ (S=1/2)	E (S=5/2) (a.u.)	$<S^2>$ (S=5/2)	ΔE (eV)
for PBE0/def2-TZVP geometries					
B3LYP/cc-pVTZ	-1538.268456	0.759	-1538.275473	8.755	-0.191
B3LYP/cc-pVTZ-DK	-1545.959098	0.759	-1545.962053	8.755	-0.080
				relativistic correction:	*0.111*
for BP86/def2-TZVP geometries					
B3LYP/cc-pVTZ	-1538.267054	0.760	-1538.273156	8.760	-0.17
B3LYP/cc-pVTZ-DK	-1545.957711	0.759	-1545.959995	8.761	-0.06
				relativistic correction:	*0.104*

Table S24: Non-relativistic and DKH2-relativistic DFT:B3LYP results for [$FeCp_2$] singlet-triplet vertical excitation energy to determine the relativistic correction.

	E (S=0) (a.u.)	E (S=1) (a.u.)	$<S^2>$ (S=1)	ΔE (eV)
for BP86/def2-TZVP geometry				
B3LYP/cc-pVTZ	-1651.009912	-1650.946817	2.031	1.717
B3LYP/cc-pVTZ-DK	-1660.079590	-1660.015882	2.030	1.734
			relativistic correction:	*0.017*
for PBE0/def2-TZVP geometry				
B3LYP/cc-pVTZ	-1651.011152	-1650.947683	2.029	1.727
B3LYP/cc-pVTZ-DK	-1660.081072	-1660.016999	2.029	1.744
			relativistic correction:	*0.016*

Table S25: Non-relativistic and DKH2-relativistic DFT:B3LYP results for [$CoCp_2$]$^+$ singlet-triplet vertical excitation energy to determine the relativistic correction.

	E (S=0) (a.u.)	E (S=1) (a.u.)	$<S^2>$ (S=1)	ΔE (eV)
for BP86/def2-TZVP geometry				
B3LYP/cc-pVTZ	-1769.862287	-1769.788324	2.058	2.013
B3LYP/cc-pVTZ-DK	-1780.494446	-1780.420675	2.057	2.007
			relativistic correction:	*-0.005*

Table S26. Detailed DFT results for [$MnCp_2$] doublet−sextet adiabatic energy.[a]

method	E (S=1/2) (a.u.)	<S²> (S=1/2)	E (S=5/2) (a.u.)	<S²> (S=5/2)	ΔE_{nrel} (eV)	ΔE [b] (eV)
for PBE0/def2-TZVP geometries						
BP86	-1538.510041	0.759	-1538.477677	8.758	0.88	0.99
BP86-D3	-1538.533370	0.759	-1538.500020	8.758	0.91	1.02
PBE	-1537.570799	0.759	-1537.535606	8.757	0.96	1.07
PBE-D3	-1537.582484	0.759	-1537.546736	8.757	0.97	1.08
PBE0	-1537.593204	0.761	-1537.606981	8.757	-0.37	-0.26
PBE0-D3	-1537.605503	0.761	-1537.618728	8.757	-0.36	-0.25
LC-wPBE	-1537.826786	0.758	-1537.820056	8.754	0.18	0.29
LC-wPBE-D3	-1537.841583	0.758	-1537.834254	8.754	0.20	0.31
PW6B95	-1539.465512	0.758	-1539.470311	8.755	-0.13	-0.02
PW6B95-D3	-1539.478809	0.758	-1539.484073	8.755	-0.14	-0.03
BLYP	-1538.161059	0.758	-1538.133708	8.755	0.74	0.85
BLYP-D3	-1538.186028	0.758	-1538.157661	8.755	0.77	0.88
B3LYP	-1538.299824	0.759	-1538.307281	8.755	-0.20	-0.09
B3LYP-D3	-1538.320189	0.759	-1538.326744	8.755	-0.18	-0.07
B3LYP*	-1537.881393	0.759	-1537.877528	8.755	0.11	0.22
B3LYP*-D3	-1537.901758	0.759	-1537.896991	8.755	0.13	0.24
B2PLYP	-1537.887408	0.759	-1537.880255	8.756	0.19	0.31
B2PLYP-D3	-1537.898443	0.759	-1537.890877	8.756	0.21	0.32
LC-BLYP	-1536.769889	0.757	-1536.766961	8.753	0.08	0.19
CAM-B3LYP	-1538.103575	0.758	-1538.112827	8.755	-0.25	-0.14
CAM-B3LYP-D3	-1538.117519	0.758	-1538.126227	8.755	-0.24	-0.13
B97D	-1538.380754	0.771	-1538.374986	8.755	0.16	0.27
wB97XD	-1538.166347	0.757	-1538.161845	8.754	0.12	0.23
OLYP	-1538.373474	0.765	-1538.364982	8.756	0.23	0.34
O3LYP	-1538.281514	0.765	-1538.292209	8.756	-0.29	-0.18
OPBE	-1538.355468	0.767	-1538.341262	8.761	0.39	0.50

(table continued on next page)

method	E (S=1/2) (a.u.)	<S²> (S=1/2)	E (S=5/2) (a.u.)	<S²> (S=5/2)	ΔE_{nrel} (eV)	ΔE [b] (eV)
(table continued from previous page)						
TPSS	-1538.432622	0.758	-1538.392954	8.758	1.08	1.19
TPSS-D3	-1538.449428	0.758	-1538.409018	8.758	1.10	1.21
TPSSh	-1538.356491	0.759	-1538.336673	8.757	0.54	0.65
TPSSh-D3	-1538.372909	0.759	-1538.352342	8.757	0.56	0.67
BR	-1538.077433	0.761	-1538.069600	8.756	0.21	0.32
LH14t-calPBE	-1536.842609	0.761	-1536.840549	8.756	0.06	0.17
LH14t-calPBE-D3	-1536.855299	0.761	-1536.852645	8.756	0.07	0.18
M06	-1537.920594	0.779	-1537.948031	8.758	-0.75	-0.64
M06-D3	-1537.923219	0.779	-1537.950537	8.758	-0.74	-0.63
M06L	-1538.207134	0.767	-1538.206323	8.763	0.02	0.13
M06L-D3	-1538.207909	0.767	-1538.207194	8.763	0.02	0.13
M11	-1537.946865	0.758	-1537.972577	8.754	-0.70	-0.59
M11L	-1538.419761	0.756	-1538.366936	8.758	1.44	1.55
MN15	-1538.153247	0.770	-1538.151534	8.757	0.05	0.16
MN15L	-1538.079609	0.803	-1538.116468	8.764	-1.00	-0.89
MVS	-5.473700	0.780	-5.492500	8.756	-0.51	-0.40
MVSh	-6.460300	0.774	-6.518300	8.756	-1.58	-1.47
SSB-D	-5.111000	0.765	-5.091200	8.756	0.54	0.65
S12h	-6.057700	0.762	-6.079200	8.756	-0.59	-0.47
S12g	-5.017300	0.763	-4.995300	8.755	0.60	0.71
for BP86/def2-TZVP geometries						
BP86	-1538.511507	0.759	-1538.479706	8.763	0.87	0.97
PBE0	-1537.591382	0.761	-1537.604199	8.763	-0.35	-0.24

[a] Single-point energy calculations for PBE0/def2-TZVP (default) or BP86/def2TZVP geometries.
[b] Best estimates, including additive relativistic correction from Table S22.

Table S27. Detailed DFT results for [$FeCp_2$], $S_0 \rightarrow T_1$ vertical excitation energy. [a]

method	E (S=0) (a.u.)	E (S=1) (a.u.)	$<S^2>$ (S=1)	ΔE_{nrel} (eV)	ΔE [b] (eV)
for BP86/def2-TZVP geometry					
BP86	-1651.290053	-1651.210963	2.027	2.15	2.17
PBE	-1650.327100	-1650.247877	2.027	2.16	2.17
PBE0	-1650.323698	-1650.266987	2.038	1.54	1.56
LC-wPBE	-1650.567226	-1650.504232	2.025	1.71	1.73
PW6B95	-1652.247099	-1652.188587	2.031	1.59	1.61
BLYP	-1650.925320	-1650.845438	2.024	2.17	2.19
B3LYP	-1651.041451	-1650.978859	2.032	1.70	1.72
B3LYP*	-1650.621806	-1650.554388	2.030	1.83	1.85
B2PLYP	-1650.647601	-1650.561563	2.038	2.34	2.36
LC-BLYP	-1649.510813	-1649.451199	2.024	1.62	1.64
CAM-B3LYP	-1650.848808	-1650.790042	2.029	1.60	1.62
B97D	-1651.220285	-1651.147613	2.049	1.98	1.99
wB97XD	-1650.911601	-1650.850037	2.027	1.68	1.69
OLYP	-1651.179841	-1651.105367	2.041	2.03	2.04
O3LYP	-1651.065691	-1651.000385	2.044	1.78	1.79
OPBE	-1651.169768	-1651.095861	2.044	2.01	2.03
TPSS	-1651.188714	-1651.109312	2.025	2.16	2.18
TPSSh	-1651.101858	-1651.031980	2.030	1.90	1.92
BR	-1650.791400	-1650.711611	2.037	2.17	2.19
LH14t-calPBE	-1649.553700	-1649.486460	2.031	1.83	1.85
M06	-1650.665507	-1650.611783	2.056	1.46	1.48
M06L	-1650.957255	-1650.890524	2.056	1.82	1.83
M11	-1650.654587	-1650.601894	2.024	1.43	1.45
M11L	-1651.176334	-1651.108629	2.015	1.84	1.86
MN15	-1650.939883	-1650.883035	2.018	1.55	1.56
MN15L	-1650.834304	-1650.772371	2.110	1.69	1.70

(table continued on next page)

method	E (S=0) (a.u.)	E (S=1) (a.u.)	$\langle S^2 \rangle$ (S=1)	ΔE_{nrel} (eV)	ΔE [b] (eV)
(table continued from previous page)					
MVS	-5.485300	-5.422779	2.093	1.70	1.72
MVSh	-6.456500	-6.412807	2.079	1.19	1.21
SSB-D	-5.124300	-5.053452	2.050	1.93	1.94
S12h	-6.056400	-6.001269	2.044	1.50	1.52
S12g	-5.031200	-4.956427	2.042	2.03	2.05
for PBE0/def2-TZVP geometry					
BP86	-1651.288433	-1651.210963	2.027	2.11	2.12
PBE0	-1650.325914	-1650.266987	2.038	1.60	1.62

[a]Single-point energy calculations for BP86/def2TZVP (default) or PBE0/def2TZVP geometry of the singlet ground state. [b] Best estimates, including additive relativistic correction from Table S23.

Table S28. Detailed DFT results for $[CoCp_2]^+$, $S_0 \rightarrow T_1$ vertical excitation energy. [a]

method	E (S=0) (a.u.)	E (S=1) (a.u.)	$<S^2>$ (S=1)	ΔE_{nrel} (eV)	ΔE [b] (eV)
BP86	-1770.157362	-1770.063977	2.025	2.54	2.54
PBE	-1769.171686	-1769.078296	2.024	2.54	2.54
PBE0	-1769.163012	-1769.096448	2.085	1.81	1.81
LC-wPBE	-1769.402546	-1769.327233	2.050	2.05	2.04
PW6B95	-1771.137604	-1771.069712	2.078	1.85	1.84
BLYP	-1769.790424	-1769.696359	2.023	2.56	2.55
B3LYP	-1769.893382	-1769.819640	2.059	2.01	2.00
B3LYP*	-1769.467675	-1769.388250	2.045	2.16	2.16
B2PLYP	-1769.500224	-1769.377393	2.328	3.34	3.34
LC-BLYP	-1768.353173	-1768.281054	2.060	1.96	1.96
CAM-B3LYP	-1769.703094	-1769.633492	2.070	1.89	1.89
B97D	-1770.163440	-1770.073643	2.039	2.44	2.44
wB97XD	-1769.764298	-1769.692759	2.060	1.95	1.94
OLYP	-1770.089197	-1769.999024	2.033	2.45	2.45
O3LYP	-1769.959224	-1769.880311	2.051	2.15	2.14
OPBE	-1770.076448	-1769.987068	2.035	2.43	2.43
TPSS	-1770.037972	-1769.946583	2.030	2.49	2.48
TPSSh	-1769.948636	-1769.868054	2.049	2.19	2.19
BR	-1769.601332	-1769.507579	2.034	2.55	2.55
LH14t-calPBE	-1768.363494	-1768.284017	2.049	2.16	2.16
M06	-1769.512690	-1769.443018	2.067	1.90	1.89
M06L	-1769.806053	-1769.728108	2.068	2.12	2.12
M11	-1769.470654	-1769.410777	2.090	1.63	1.62
M11L	-1770.020879	-1769.946366	2.035	2.03	2.02
MN15	-1769.827207	-1769.754010	2.017	1.99	1.99
MN15L	-1769.696323	-1769.617886	2.091	2.13	2.13
MVS	-5.222617	-5.145268	2.078	2.10	2.10
MVSh	-6.176189	-6.125421	2.205	1.38	1.38
SSB-D	-4.863020	-4.779041	2.044	2.29	2.28
S12h	-5.784259	-5.720141	2.095	1.74	1.74
S12g	-4.775035	-4.686103	2.035	2.42	2.41

[a] Single-point energy calculations for BP86/def2-TZVP geometry of the singlet ground state.
[b] Best estimates, including additive relativistic correction from Table S24.

Table S29. Detailed DFT results for [$RuCp_2$], $S_0 \rightarrow T_1$ vertical excitation energy. [a]

method	E (S=0) (a.u.)	E (S=1) (a.u.)	$\langle S^2 \rangle$ (S=1)	ΔE(eV)
for BP86/def2-TZVP geometry				
BP86	-482.364909	-482.239488	2.009	3.41
PBE	-481.756438	-481.630970	2.009	3.41
PBE0	-481.748926	-481.628289	2.013	3.28
LC-wPBE	-481.965017	-481.845915	2.011	3.24
PW6B95	-482.783818	-482.661033	2.010	3.34
BLYP	-482.000446	-481.875459	2.008	3.40
B3LYP	-482.238070	-482.116269	2.011	3.31
B3LYP*	-481.956779	-481.833717	2.010	3.35
B2PLYP	-481.903844	-481.772301	2.019	3.58
LC-BLYP	-480.821376	-480.703178	2.011	3.22
CAM-B3LYP	-481.931925	-481.811799	2.011	3.27
B97D	-482.134380	-482.011456	2.013	3.34
wB97XD	-482.111676	-481.989106	2.011	3.34
OLYP	-482.188485	-482.064966	2.010	3.36
O3LYP	-482.191179	-482.069372	2.011	3.31
OPBE	-482.313493	-482.189074	2.011	3.39
TPSS	-482.298324	-482.169571	2.010	3.50
TPSSh	-482.242406	-482.116227	2.011	3.43
BR	-482.140249	-482.011910	2.011	3.49
LH14t-calPBE	-481.454845	-481.338042	2.010	3.18
M06	-481.911682	-481.792444	2.013	3.24
M06L	-482.239698	-482.115108	2.016	3.39
M11	-481.859801	-481.740235	2.010	3.25
M11L	-482.388713	-482.277358	2.021	3.03
MN15	-481.799540	-481.675348	2.006	3.38
MN15L	-481.720362	-481.595437	2.022	3.40
MVS	-5.467267	-5.350355	2.023	3.18
MVSh	-6.392441	-6.279717	2.024	3.07
SSB-D	-5.100782	-4.982225	2.012	3.23
S12h	-5.989855	-5.872781	2.014	3.19
S12g	-5.007957	-4.887381	2.011	3.28
for PBE0/def2-TZVP geometry				
BP86	-482.364909	-482.232830	2.008	3.59
PBE0	-481.751265	-481.625058	2.012	3.43

[a] Single-point energy calculations for BP86/def2TZVP (default) or PBE0/def2TZVP geometry of the singlet ground state.

Table S30. Detailed DFT results for [$RuCp_2$] S_0 − T_1 adiabatic energy. [a]

method	E (S=0) (a.u.)	E (S=1) (a.u.)	$\langle S^2 \rangle$ (S=1)	ΔE (eV)
for PBE0/def2-TZVP geometries				
BP86	-482.364909	-482.263517	2.011	2.76
PBE0	-481.751265	-481.653292	2.019	2.67
for BP86/def2-TZVP geometries				
BP86	-482.364909	-482.267604	2.011	2.65
BP86-D3	-482.382585	-482.285080	2.011	2.65
PBE	-481.756438	-481.656761	2.011	2.71
PBE-D3	-481.765677	-481.665873	2.011	2.72
PBE0	-481.748926	-481.650713	2.020	2.67
PBE0-D3	-481.758421	-481.660115	2.020	2.68
LC-wPBE	-481.965017	-481.863510	2.021	2.76
LC-wPBE-D3	-481.976126	-481.874540	2.021	2.76
PW6B95	-482.783818	-482.684093	2.015	2.71
PW6B95-D3	-482.798611	-482.698559	2.015	2.72
BLYP	-482.000446	-481.910831	2.010	2.44
BLYP-D3	-482.019331	-481.929492	2.010	2.44
B3LYP	-482.238070	-482.147367	2.016	2.47
B3LYP-D3	-482.253370	-482.162554	2.016	2.47
B3LYP*	-481.956779	-481.864251	2.014	2.52
B3LYP*-D3	-481.972079	-481.879438	2.014	2.52
B2PLYP	-481.903844	-481.797686	2.034	2.89
B2PLYP-D3	-481.911977	-481.805777	2.034	2.89
LC-BLYP	-480.821376	-480.722098	2.021	2.70
CAM-B3LYP	-481.931925	-481.838355	2.018	2.55
CAM-B3LYP-D3	-481.942379	-481.848735	2.018	2.55
B97D	-482.134380	-482.039705	2.016	2.58
wB97XD	-482.111676	-482.011690	2.018	2.72
OLYP	-482.188485	-482.089678	2.013	2.69
O3LYP	-482.191179	-482.093131	2.016	2.67
OPBE	-482.313493	-482.204894	2.014	2.96
TPSS	-482.298324	-482.196774	2.013	2.76
TPSS-D3	-482.311318	-482.209596	2.013	2.77
TPSSh	-482.242406	-482.141535	2.016	2.74
TPSSh-D3	-482.254998	-482.153998	2.016	2.75

(table continued on next page)

method	E (S=0) (a.u.)	E (S=1) (a.u.)	$\langle S^2 \rangle$ (S=1)	ΔE (eV)
(table continued from previous page)				
BR	-482.140249	-482.049275	2.013	2.48
LH14t-calPBE	-481.454845	-481.351971	2.014	2.80
LH14t-calPBE-D3	-481.464831	-481.361820	2.014	2.80
M06	-481.911682	-481.817805	2.020	2.55
M06-D3	-481.914201	-481.820254	2.020	2.56
M06L	-482.239698	-482.137524	2.022	2.78
M06L-D3	-482.240496	-482.138320	2.022	2.78
M11	-481.859801	-481.765228	2.015	2.57
M11L	-482.388713	-482.299598	2.026	2.42
MN15	-481.799540	-481.698239	2.010	2.76
MN15L	-481.720362	-481.619481	2.028	2.75
MVS	-5.467267	-5.370290	2.028	2.64
MVSh	-6.392441	-6.299210	2.036	2.54
SSB-D	-5.100782	-4.997950	2.016	2.80
S12h	-5.989855	-5.895663	2.021	2.56
S12g	-5.007957	-4.908796	2.013	2.70

[a] Single-point energy calculations for BP86/def2TZVP (default) or PBE0/def2TZVP geometries.

Table S31. Detailed DFT results for [$RuCp_2$], $T_1 \rightarrow S_0$ vertical emission energy.[a]

method	E (S=0) (a.u.)	E (S=1) (a.u.)	$\langle S^2 \rangle$ (S=1)	ΔE (eV)
for BP86/def2-TZVP geometry				
BP86	-482.31211408466	-482.267604	2.011	1.21
PBE0	-481.68953084271	-481.650713	2.020	1.06
for PBE0/def2-TZVP geometry				
BP86	-482.33643126559	-482.263517	2.011	1.98
PBE0	-481.71763022531	-481.653292	2.019	1.75
for UHF-CCSD(T)/cT(D)-PP geometry				
BP86	-482.339565	-482.264199	2.012	2.05
PBE	-481.728846	-481.653044	2.011	2.06
PBE0	-481.718844	-481.652479	2.020	1.81
LC-wPBE	-481.929687	-481.866894	2.021	1.71
PW6B95	-482.756239	-482.686756	2.015	1.89
BLYP	-481.985113	-481.908647	2.010	2.08
B3LYP	-482.219070	-482.149665	2.016	1.89
B3LYP*	-481.936848	-481.865202	2.014	1.95
B2PLYP	-481.876114	-481.798699	2.033	2.11
LC-BLYP	-480.790348	-480.727675	2.021	1.71
CAM-B3LYP	-481.908287	-481.842558	2.018	1.79
B97D	-482.109870	-482.036175	2.016	2.01
wB97XD	-482.083257	-482.014027	2.018	1.88
OLYP	-482.159902	-482.086787	2.014	1.99
O3LYP	-482.162547	-482.092783	2.016	1.90
OPBE	-482.272875	-482.200890	2.015	1.96
TPSS	-482.270578	-482.195750	2.014	2.04
TPSSh	-482.213608	-482.142580	2.017	1.93
BR	-482.125751	-482.047260	2.013	2.14
LH14t-calPBE	-481.425086	-481.352421	2.015	1.98
M06	-481.887905	-481.816688	2.018	1.94
M06L	-482.207418	-482.138136	2.026	1.89
M11	-481.834446	-481.769452	2.014	1.77
M11L	-482.362877	-482.302039	2.026	1.66
MN15	-481.770884	-481.697155	2.010	2.01
MN15L	-481.686127	-481.616599	2.031	1.89
MVS	-5.433496	-5.368752	2.030	1.76
MVSh	-6.359103	-6.302083	2.037	1.55
SSB-D	-5.064722	-4.995379	2.016	1.89
S12h	-5.961737	-5.898170	2.021	1.73
S12g	-4.977739	-4.905795	2.014	1.96

a Single-point calculations for BP86/def2TZVP, PBE0/def2TZVP or UHF-CCSD(T)/cT(D)-PP (default) geometry of T1 excited state

Table S32. Cross-check of selected DFT results from different programs: [$MnCp_2$], doublet−sextet adiabatic energy (using PBE0/def2-TZVP geometries).

method	basis set	program	S=1/2	S=5/2	ΔE (eV)
PBE	ET-pVQZ(TZ2P)	ADF2017	-4.95469787	-4.92039338	0.93
	def2-QZ(T)VPP	Turbomole7	-1537.570799	-1537.535606	0.96
PBE0	ET-pVQZ(TZ2P)	ADF2017	-6.07556432	-6.09059086	-0.41
	def2-QZ(T)VPP	G16	-1537.593204	-1537.606981	-0.37
	def2-QZ(T)VPP	Turbomole7	-1537.593204	-1537.606981	-0.37
M06	ET-pVQZ(TZ2P)	ADF2017	-5.89309694	-5.91904658	-0.71
	def2-QZ(T)VPP	G16	-1537.920594	-1537.948031	-0.75

Table S33. Cross-check of selected DFT results from different programs: [$FeCp_2$], singlet−triplet vertical excitation energy (using BP86/def2-TZVP geometry of singlet).

method	basis set	program	S=0	S=1	ΔE (eV)
PBE	ET-pVQZ(TZ2P)	ADF2017	-4.96794343	-4.88821933	2.17
	def2-QZ(T)VPP	Turbomole	-1650.327100	-1650.247877	2.16
PBE0	ET-pVQZ(TZ2P)	ADF2017	-6.07401023	-6.01692879	1.55
	def2-QZ(T)VPP	Turbomole	-1650.323698	-1650.266987	1.54
M06	ET-pVQZ(TZ2P)	ADF2017	-5.90181502	-5.84757295	1.48
	def2-QZ(T)VPP	G16	-1650.665507	-1650.611783	1.46

Table S34. Cross-check of selected DFT results from different programs:$[CoCp2]^{+}$, singlet−triplet vertical excitation energy (using BP86/def2-TZVP geometry of singlet).

method	basis set	program	S=0	S=1	ΔE (eV)
PBE	ET-pVQZ(TZ2P)	ADF2017	-4.71268819	-4.61932038	2.54
	def2-QZ(T)VPP	Turbomole7	-1769.171686	-1769.078296	2.54
PBE0	ET-pVQZ(TZ2P)	ADF2017	-5.80115795	-5.73480554	1.81
	def2-QZ(T)VPP	Turbomole	-1769.163012	-1769.096448	1.81
M06	ET-pVQZ(TZ2P)	ADF2017	-5.63388678	-5.56437829	1.89
	def2-QZ(T)VPP	G16	-1769.512690	-1769.443018	1.90

Table S35. Cross-check of selected DFT results from different programs: $[RuCp_2]$, singlet−triplet adiabatic energy (using BP86/def2-TZVP geometries).

method	basis set	program	S=0	S=1	ΔE (eV)
PBE	ZORA/QZ4P(TZ2P)	ADF2017	-4.95148669	-4.85382699	2.66
	def2-QZ(T)VPP	Turbomole7	-481.756438	-481.656761	2.71
PBE0	ZORA/QZ4P(TZ2P)	ADF2017	-6.01292217	-5.91682351	2.61
	def2-QZ(T)VPP	Turbomole7	-481.748926	-481.650713	2.67
M06	ZORA/QZ4P(TZ2P)	ADF2017	-5.84202873	-5.74980101	2.51
	def2-QZ(T)VPP	G16	-481.911682	-481.817805	2.55

Table S36. Cross-check of selected DFT results from different programs: $[RuCp_2]$, singlet−triplet vertical excitation energy (using BP86/def2-TZVP geometry of singlet).

method	basis set	program	S=0	S=1	ΔE (eV)
PBE	ZORA/QZ4P(TZ2P)	ADF2017	-4.95148669	-4.82653980	3.40
	def2-QZ(T)VPP	Turbomole7	-481.756438	-481.630970	3.41
PBE0	ZORA/QZ4P(TZ2P)	ADF2017	-6.01292217	-5.89317248	3.26
	def2-QZ(T)VPP	Turbomole7	-481.748926	-481.628289	3.28
M06	ZORA/QZ4P(TZ2P)	ADF2017	-5.84202873	-5.72372797	3.22
	def2-QZ(T)VPP	G16	-481.911682	-481.792444	3.24

Table S37. Estimate of solvation effects on DFT adiabatic energy (doublet - sextet) for $MnCp_2$.

	Total energies (a.u.) [a]		ΔE (eV)
	S=1/2	S=5/2	
gas/gas [b]	-1537.546287	-1537.560639	**-0.391**
solv/gas [c]	-1537.549697	-1537.564256	-0.396
gas/solv [d]	-1537.549561	-1537.564274	-0.400
solv/solv [e]	-1537.546144	-1537.560623	**-0.394**
		estimated solvation effect [f]	-0.003

[a] PBE0/def2-TZVP total energies calculated either in gas phase or within the COSMO model (toluene, ε=2.4). [b] Energy calculations in gas phase for geometry optimized in gas phase; [c] Energy calculations in solvent for geometry optimized in gas phase; [d] Energy calculations in gas phase for geometry optimized in solvent. [e] Energy calculations in solvent for geometry optimized in solvent. [f] Difference between ΔE values for solvated (solv/solv) and unsolvated (gas/gas) model, the values subtracted are boldfaced.

5. Detailed coupled cluster results

Table S38. Detailed coupled cluster results for [$MnCp_2$] doublet−sextet adiabatic energy. [a]

basis set	theory level	E (S=1/2) (a.u.)	E (S=5/2) (a.u.)	ΔE (eV)
for PBE0/def2-TZVP geometries:				
cT(D)-DK	ROHF	-1541.952163	-1542.120173	-4.57
	RCCSD	-1544.281133	-1544.312201	-0.85
	UCCSD	-1544.281956	-1544.313464	-0.86
	RCCSD(T)	-1544.416091	-1544.419971	-0.11
	UCCSD(T)	-1544.416884	-1544.421220	-0.12
	UCCSD(T) frozen 3s3p	-1543.995425	-1544.009674	-0.39
	KS-RCCSD	-1544.251345	-1544.292350	-1.12
	KS-UCCSD	-1544.252001	-1544.293866	-1.14
	KS-RCCSD(T)	-1544.410268	-1544.410133	0.00
	KS-UCCSD(T)	-1544.410725	-1544.411188	-0.01
cT(D)-NR	ROHF	-1534.296958	-1534.470208	-4.71
	RCCSD	-1536.624580	-1536.660399	-0.97
	UCCSD	-1536.625412	-1536.661666	-0.99
	RCCSD(T)	-1536.759393	-1536.767880	-0.23
	UCCSD(T)	-1536.760195	-1536.769137	-0.24
	KS-RCCSD(T)	-1536.753694	-1536.758164	-0.12
	KS-UCCSD(T)	-1536.754159	-1536.759231	-0.14
	RCCSD(T*)-F12a	-1537.004918	-1537.003089	0.05
	UCCSD(T*)-F12a	-1537.005716	-1537.004368	0.04
	KS-RCCSD(T*)-F12a	-1536.995400	-1536.989726	0.15
	KS-UCCSD(T*)-F12a	-1536.995848	-1536.990710	0.14
for BP86/def2-TZVP geometries:				
cT(D)-DK	UCCSD(T)	-1544.417464	-1544.420044	-0.07
cT(D)-NR	UCCSD(T)	-1536.760773	-1536.767682	-0.19
	UCCSD(T*)-F12a	-1537.005499	-1537.002502	0.08

[a] Single point calculations for PBE0/def2-TZVP (default) or BP86/def2-TZVP geometries.

Table S39. Detailed coupled cluster results for [$FeCp_2$], $S_0 \rightarrow T_1$ vertical excitation energy. [a]

basis set	theory level	E (S=0) (a.u.)	E (S=1) (a.u.)	ΔE (eV)
for BP86/def2-TZVP geometry:				
cT(D)-DK	RHF/ROHF	-1655.929466	-1655.920218	0.25
	RCCSD	-1658.378913	-1658.312237	1.81
	UCCSD	-1658.378913	-1658.315383	1.73
	RCCSD(T)	-1658.527123	-1658.447800	2.16
	UCCSD(T)	-1658.527123	-1658.450771	2.08
	UCCSD(T) Frozen 3s3p	-1658.099281	-1658.023483	2.06
	KS-RCCSD	-1658.341715	-1658.283818	1.58
	KS-UCCSD	-1658.341715	-1658.286078	1.51
	KS-RCCSD(T)	-1658.517558	-1658.443880	2.00
	KS-UCCSD(T)	-1658.517558	-1658.445219	1.97
cT(D)-NR	RHF/ROHF	-1646.898635	-1646.890496	0.22
	RCCSD	-1649.346594	-1649.280627	1.80
	UCCSD	-1649.346594	-1649.283791	1.71
	RCCSD(T)	-1649.494659	-1649.415923	2.14
	UCCSD(T)	-1649.494659	-1649.418907	2.06
	KS-RCCSD(T)	-1649.485136	-1649.412070	1.99
	KS-UCCSD(T)	-1649.485136	-1649.413420	1.95
	RCCSD(T*)-F12a	-1649.752709	-1649.671066	2.22
	UCCSD(T*)-F12a	-1649.752709	-1649.674065	2.14
	KS-RCCSD(T*)-F12a	-1649.739471	-1649.663928	2.06
	KS-UCCSD(T*)-F12a	-1649.739471	-1649.665126	2.02
for PBE0/def2-TZVP geometry:				
cT(D)-DK	UCCSD(T)	-1658.526375	-1658.449955	2.08
cT(D)-NR	UCCSD(T)	-1649.493842	-1649.418017	2.06
	UCCSD(T*)-F12a	-1649.752770	-1649.674050	2.14

[a] Single point calculations for BP86/def2-TZVP (default) or PBE0/def2-TZVP geometry of the singlet ground state.

Table S40. Detailed coupled cluster results for $[CoCp_2]^+$, $S_0 \rightarrow T_1$ vertical excitation energy. [a]

basis set	theory level	E (S=0) (a.u.)	E (S=1) (a.u.)	ΔE (eV)
cT(D)-DK	RHF/ROHF	-1776.267725	-1776.253807	0.38
	RCCSD	-1778.764657	-1778.688158	2.08
	UCCSD	-1778.764657	-1778.692682	1.96
	RCCSD(T)	-1778.915315	-1778.826790	2.41
	UCCSD(T)	-1778.915315	-1778.830249	2.31
	UCCSD(T) Frozen 3s3p	-1778.484817	-1778.400683	2.29
	KS-RCCSD	-1778.729395	-1778.661983	1.83
	KS-UCCSD	-1778.729395	-1778.665024	1.75
	KS-RCCSD(T)	-1778.906300	-1778.822767	2.27
	KS-UCCSD(T)	-1778.906300	-1778.824249	2.23
cT(D)-NR	RHF/ROHF	-1765.676477	-1765.662886	0.37
	RCCSD	-1768.173121	-1768.096430	2.09
	UCCSD	-1768.173121	-1768.101067	1.96
	RCCSD(T)	-1768.323867	-1768.234982	2.42
	UCCSD(T)	-1768.323867	-1768.238540	2.32
	KS-RCCSD(T)	-1768.315084	-1768.231350	2.28
	KS-UCCSD(T)	-1768.315084	-1768.232843	2.24
	RCCSD(T*)-F12a	-1768.588650	-1768.496662	2.50
	UCCSD(T*)-F12a	-1768.588650	-1768.500094	2.41
	KS-RCCSD(T*)-F12a	-1768.576853	-1768.490041	2.36
	KS-UCCSD(T*)-F12a	-1768.576853	-1768.491318	2.33

[a] Single point calculations for BP86/def2-TZVP geometry of the singlet ground state.

Table S41. Detailed coupled cluster results for $RuCp_2$, S_0 - T_1 adiabatic energy. [a]

basis set	theory level	E (S=0) (a.u.)	E (S=1) (a.u.)	ΔE (eV)
for BP86/def2-TZVP geometries:				
cT(D)-PP	RHF/ROHF	-478.421507	-478.358552	1.71
	RCCSD	-480.762873	-480.663789	2.70
	UCCSD	-480.762873	-480.666438	2.62
	RCCSD(T)	-480.902896	-480.797655	2.86
	UCCSD(T)	-480.902896	-480.800098	2.80
	UCCSD(T) Frozen 4s4p	-480.515076	-480.412092	2.80
	KS-RCCSD(T)	-480.895357	-480.794783	2.74
	KS-UCCSD(T)	-480.895357	-480.795715	2.71
	RCCSD(T*)-F12a	-481.174697	-481.066179	2.95
	UCCSD(T*)-F12a	-481.174697	-481.068698	2.88
	KS-RCCSD(T*)-F12a	-481.163824	-481.060519	2.81
	KS-UCCSD(T*)-F12a	-481.163824	-481.061360	2.79
for PBE0/def2-TZVP geometries:				
cT(D)-PP	UCCSD(T)	-480.902526	-480.800439	2.78
	UCCSD(T*)-F12a	-481.175302	-481.069244	2.89

[a] Single-point calculations for BP86/def2TZVP (default) or PBE0/def2-TZVP geometries.

Table S42. Detailed coupled cluster results for $RuCp_2$, $S_0 \rightarrow T_1$ vertical excitation energy. [a]

basis set	theory level	E (S=0) (a.u.)	E (S=1) (a.u.)	ΔE (eV)
for BP86/def2-TZVP geometry:				
cT(D)-PP	RHF/ROHF	-478.421507	-478.319711	2.77
	RCCSD	-480.762873	-480.639089	3.37
	UCCSD	-480.762873	-480.641063	3.31
	RCCSD(T)	-480.902896	-480.773593	3.52
	UCCSD(T)	-480.902896	-480.775252	3.47
	UCCSD(T) Frozen 4s4p	-480.515076	-480.386702	3.49
	KS-RCCSD(T)	-480.895357	-480.769837	3.42
	KS-UCCSD(T)	-480.895357	-480.770518	3.40
	RCCSD(T*)-F12a	-481.174697	-481.043682	3.57
	UCCSD(T*)-F12a	-481.174697	-481.045401	3.52
	KS-RCCSD(T*)-F12a	-481.163824	-481.036975	3.45
	KS-UCCSD(T*)-F12a	-481.163824	-481.037522	3.44
for PBE0/def2-TZVP geometry:				
cT(D)-PP	UCCSD(T)	-480.902526	-480.769053	3.63
	UCCSD(T*)-F12a	-481.175302	-481.040244	3.68

[a] Single-point calculations for BP86/def2TZVP (default) or PBE0/def2-TZVP geometry of the singlet ground state.

Table S43. Detailed Results of CC calculations for $RuCp_2$, $T_1 \rightarrow S_0$ vertical emission energy. [a]

basis set	theory level	E (S=0) (a.u.)	E (S=1) (a.u.)	ΔE (eV)
for PBE0/def2-TZVP geometry:				
cT(D)-PP	UCCSD(T)	-480.871577	-480.800439	1.94
	UCCSD(T*)-F12a	-481.142646	-481.069244	2.00
for BP86/def2-TZVP geometry:				
cT(D)-PP	UCCSD(T)	-480.847008	-480.800098	1.28
	UCCSD(T*)-F12a	-481.117551	-481.068698	1.33
for UHF-CCSD(T)/cT(D)-PP geometry:				
cT(D)-PP	RHF/ROHF	-478.416745	-478.371997	1.22
	RCCSD	-480.736315	-480.668191	1.85
	UCCSD	-480.736315	-480.669942	1.81
	RCCSD(T)	-480.874270	-480.799624	2.03
	UCCSD(T)	-480.874270	-480.801138	1.99
	UCCSD(T) Frozen 4s4p	-480.486485	-480.413205	1.99
	KS-RCCSD(T)	-480.867009	-480.794935	1.96
	KS-UCCSD(T)	-480.867009	-480.795846	1.94
	RCCSD(T*)-F12a	-481.144831	-481.067908	2.09
	UCCSD(T*)-F12a	-481.144831	-481.069417	2.05
	KS-RCCSD(T*)-F12a	-481.134396	-481.060209	2.02
	KS-UCCSD(T*)-F12a	-481.134396	-481.061042	2.00

[a] Single-point calculations for PBE0/def2-TZVP, BP86/def2TZVP or UHF-CCSD(T)/cT(D)-PP (default) geometry of the triplet excited state.

6. Active orbitals

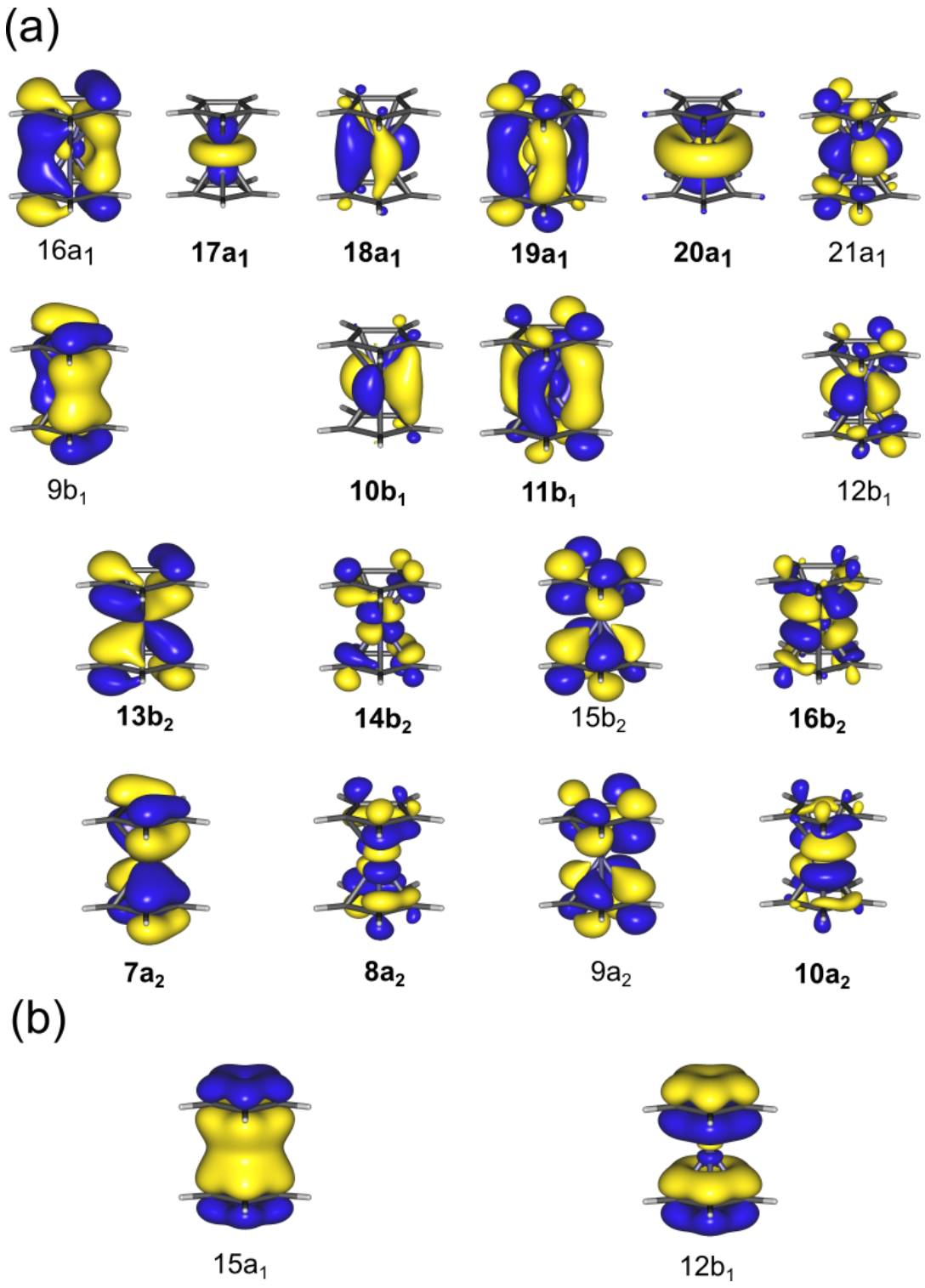

Figure S8. Contour plots of CASSCF natural orbitals for [$FeCp_2$] in singlet ground state. (a) Orbitals of the (14,18) active space, those with bold labels are included in the (10,12) active space; (b) additional orbitals included only in the (18,15) active space. Contour value ±0.04 au.

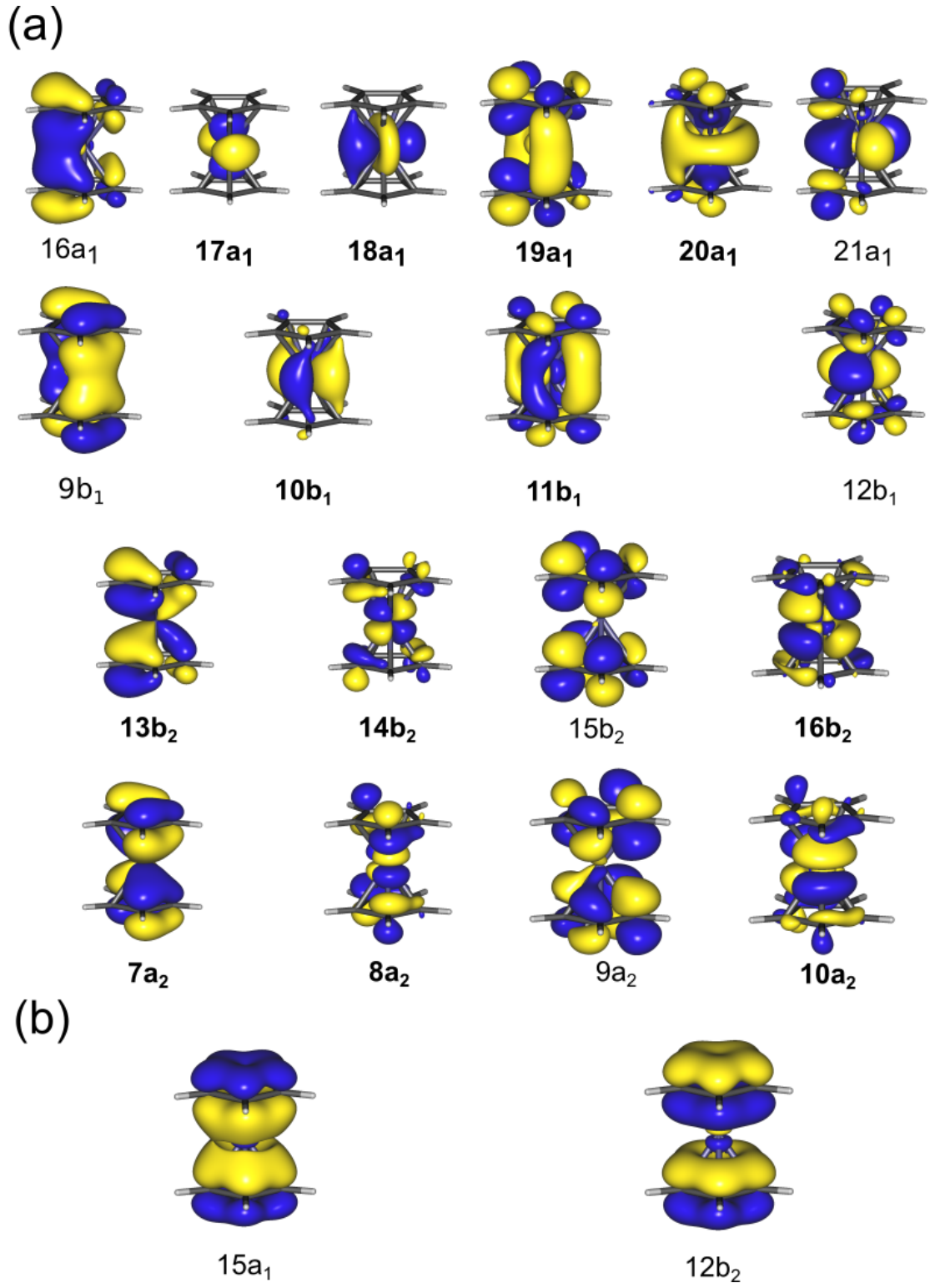

Figure S9. Contour plots of CASSCF natural orbitals for [$FeCp_2$] in the lowest triplet excited state (state-specific calculations for one component of T_1). (a) Orbitals of the (14,18) active space, those with bold labels are included in the (10,12) active space; (b) additional orbitals included only in the (18,15) active space. Contour value ±0.04 au.

Table S44. Natural orbital occupation numbers for active orbitals corresponding to difference choices of the active space for [$FeCp_2$] in the singlet ground state (S_0) and the lowest triplet excited (T_1) state computed vertically for the S_0 geometry.

	(14,18)		(18,15)		(14,16)		(10,14)		(10,12)		(10,10)	
	S_0	T_1	S_0	T_1	S_0	T_1	S_0	T_1	S_0	T_1	S_0	T_1
15a1	–	–	1.988	1.988	–	–	–	–	–	–	–	–
16a1	1.968	1.961	1.968	1.973	1.970	1.961	–	–	–	–	–	–
17a1	1.910	1.953	1.996	1.021	1.966	1.954	1.967	1.945	1.964	1.959	1.963	1.958
18a1	1.910	1.001	1.907	1.919	1.915	0.992	1.919	1.037	1.931	1.063	1.934	0.998
19a1	0.079	0.066	0.088	0.089	0.077	0.065	0.063	0.048	0.052	0.036	0.053	0.039
20a1	0.028	0.021	–	–	0.029	0.026	0.027	0.013	0.030	0.016	0.032	0.016
21a1	0.005	0.006	–	–	0.005	0.008	0.003	0.003	–	–	–	–
9b1	1.968	1.965	1.968	1.966	1.970	1.968	–	–	–	–	–	–
10b1	1.910	1.914	1.907	1.893	1.915	1.925	1.919	1.885	1.931	1.874	1.934	1.933
11b1	0.079	0.071	0.088	0.094	0.077	0.070	0.063	0.058	0.052	0.043	0.053	0.049
12b1	0.005	0.006	–	–	0.005	0.007	0.003	0.003	–	–	–	–
12b2	–	–	1.983	1.983	–	–	–	–	–	–	–	–
13b2	1.916	1.945	1.919	1.954	1.923	1.946	1.933	1.974	1.941	1.937	1.948	1.982
14b2	0.096	0.998	0.095	1.006	0.085	1.008	0.083	0.969	0.077	0.146	0.087	1.010
15b2	0.029	0.043	0.039	0.042	0.028	0.043	0.001	0.008	0.001	0.002	–	–
16b2	0.002	0.008	–	–	–	–	–	–	–	–	–	–
7a2	1.916	1.904	1.919	1.892	1.923	1.911	1.933	1.924	1.941	1.976	1.948	1.940
8a2	0.096	0.108	0.095	0.141	0.085	0.093	0.083	0.132	0.077	0.938	0.067	0.081
9a2	0.029	0.025	0.039	0.043	0.028	0.023	0.002	0.002	0.001	0.009	–	–
10a2	0.002	0.002	–	–	–	–	–	–	–	–	–	–

"–" means that given orbital is not included (inactive or secondary) for a given active space.

7. Detailed multiconfigurational results

Table S45. Detailed multiconfigurational results for [$MnCp_2$] doublet−sextet adiabatic energy. [a]

	E (S=1/2) (a.u.)	E (S=5/2) (a.u.)	ΔE (eV)
CASSCF(9,12)	-1542.103230	-1542.167382	-1.75
CASPT2(9,12)	-1544.304084	-1544.301667	0.07
CASPT2(9,12) Frozen 3s3p	-1543.882263	-1543.887679	-0.15
pc-NEVPT2(9,12)	-1544.266035	-1544.244897	0.58
sc-NEVPT2(9,12)	-1544.254798	-1544.238062	0.46
MRCISD(9,12)	-1543.686614	-1543.711428	-0.68
MRCISD+Q(D)(9,12) [b]	-1544.126685	-1544.138207	-0.31
MRCISD+Q(DS)(9,12) [b]	-1544.296072	-1544.301230	-0.14
MRCISD+Q(P)(9,12) [b]	-1544.272246	-1544.278265	-0.16
C_0 [c]	0.884599	0.885128	

[a] Single-point calculations for PBE0/def2-TZVP structures, using the cT(D)-DK basis set. [b] Energies including Davidson (D), Davidson-Silver (DS), or Pople (P) size-extensivity correction (fixed reference). [c] Coefficient of the reference function in the MRCISD wave function (fixed reference) used for determining size-extensivity corrections.

Table S46. Detailed multiconfigurational results for [$FeCp_2$], $S_0 \rightarrow T_1$ vertical excitation energy. [a]

	E (S=0) (a.u.)	E (S=1) (a.u.)	ΔE (eV)
CASSCF(10,12)	-1656.152212	-1656.081998	1.91
CASPT2(10,12)	-1658.420670	-1658.346359	2.02
CASPT2(10,12) Frozen 3s3p	-1657.988749	-1657.913720	2.04
pc-NEVPT2(10,12)	-1658.380034	-1658.292827	2.37
sc-NEVPT2(10,12)	-1658.366528	-1658.280191	2.35
MRCISD(10,12)	-1657.777165	-1657.703989	1.99
MRCISD+Q(D)(10,12) [b]	-1658.224300	-1658.150229	2.02
MRCISD+Q(DS)(10,12) [b]	-1658.394047	-1658.319594	2.03
MRCISD+Q(P)(10,12) [b]	-1658.370105	-1658.295705	2.02
C_0 [c]	0.885556	0.885574	

[a] Single-point calculations for BP86/def2-TZVP structure of the singlet ground state, using the cT(D)-DK basis set.
[b] Energies including Davidson (D), Davidson-Silver (DS), or Pople (P) size-extensivity correction (fixed reference).
[c] Coefficient of the reference function in the MRCISD wave function (fixed reference) used for determining size-extensivity corrections.

Table S47. Detailed multiconfigurational results for $[CoCp_2]^+$, $S_0 \rightarrow T_1$ vertical excitation energy. [a,]

	E (S=0) (a.u.)	E (S=1) (a.u.)	ΔE (eV)
CASSCF(10,12)	-1776.542524	-1776.463180	2.16
CASPT2(10,12)	-1778.808319	-1778.720571	2.39
CASPT2(10,12) Frozen 3s3p	-1778.373244	-1778.286428	2.36
pc-NEVPT2(10,12)	-1778.752332	-1778.653838	2.68
sc-NEVPT2(10,12)	-1778.735519	-1778.637612	2.66
MRCISD(10,12)	-1778.179353	-1778.094994	2.30
MRCISD+Q(D)(10,12) [b]	-1778.618071	-1778.532713	2.32
MRCISD+Q(DS)(10,12) [b]	-1778.778718	-1778.693167	2.33
MRCISD+Q(P)(10,12) [b]	-1778.755886	-1778.670368	2.33
C_0 [c]	0.888046	0.887972	

[a] Single-point calculations for BP86/def2-TZVP structure of the singlet ground state, using the cT(D)-DK basis set.
[b] Energies including Davidson (D), Davidson-Silver (DS), or Pople (P) size-extensivity correction (fixed reference).
[c] Coefficient of the reference function in the MRCISD wave function (fixed reference) used for determining size-extensivity corrections.

Table S48. Detailed multiconfigurational results for [$RuCp_2$], $S_0 - T_1$ adiabatic energy. [a,]

	E (S=0) (a.u.)	E (S=1) (a.u.)	ΔE (eV)
CASSCF(10,12)fix [b]	-478.541623	-478.449789	2.50
CASPT2(10,12)fix [b]	-480.804256	-480.691941	3.06
CASPT2(10,12)fix Frozen 4s4p [b]	-480.417061	-480.303605	3.09
pc-NEVPT2(10,12)fix [b]	-480.788554	-480.653236	3.68
sc-NEVPT2(10,12)fix [b]	-480.778994	-480.644669	3.66
MRCISD(10,12)fix [b]	-480.127947	-480.025801	2.78
MRCISD+Q(D)(10,12)fix [b,c]	-480.591801	-480.487579	2.84
MRCISD+Q(DS)(10,12)fix [b,c]	-480.783485	-480.678957	2.84
MRCISD+Q(P)(10,12)fix [b,c]	-480.745155	-480.640706	2.84
C_0 [d]	0.879630	0.879427	

[a] Single-point calculations for BP86/def2-TZVP structures, using the cT(D)-PP basis set. [b] "(10,12)fix" means that double-shell orbitals d'xz and d'yz were taken from CASSCF(10,12) state-average calculations of six lowest triplet roots (all components of the T_1, T_2, T_3 states) and not optimized any further. [c] Energies including Davidson (D), Davidson-Silver (DS), or Pople (P) size-extensivity correction (fixed reference). [d] Coefficient of the reference function in the MRCISD wave function (fixed reference) used for determining size-extensivity corrections.

Table S49. Detailed multiconfigurational results for [$RuCp_2$], $S_0 \rightarrow T_1$ vertical excitation energy. [a]

	E (S=0) (a.u.)	E (S=1) (a.u.)	ΔE (eV)
CASSCF(10,12) [b]	-478.541984	-478.413088	3.51
CASSCF(10,12)fix [c]	-478.541623	-478.413041	3.50
CASPT2(10,12) [b]	-480.804375	-480.679426	3.40
CASPT2(10,12)fix [c]	-480.804256	-480.679518	3.39
CASPT2(10,12) Frozen 4s4p [b]	-480.417246	-480.289302	3.48
pc-NEVPT2(10,12)fix [c]	-480.788554	-480.655757	3.61
sc-NEVPT2(10,12)fix [c]	-480.778994	-480.645470	3.63
MRCISD(10,12)fix [c]	-480.127947	-479.999918	3.48
MRCISD+Q(D)(10,12)fix [c,d]	-480.591801	-480.464195	3.47
MRCISD+Q(DS)(10,12)fix [c,d]	-480.783485	-480.656206	3.46
MRCISD+Q(P)(10,12)fix [c,d]	-480.745155	-480.617816	3.47
C_0 [e]	0.879630	0.879574	

[a] Single-point calculations for BP86/def2-TZVP structure of the singlet ground state, using the cT(D)-PP basis set. [b] CASSCF(10,12) for S_0 state could be converged to desired solution only with Molcas. [c] "(10,12)fix" means that double-shell orbitals d'xz and d'yz were taken from CASSCF(10,12) state-average calculations of six lowest triplet roots (all components of the T_1, T_2, T_3 states) and not optimized any further. [d] Energies including Davidson (D), Davidson-Silver (DS), or Pople (P) size-extensivity correction (fixed reference). [e] Coefficient of the reference function in the MRCISD wave function (fixed reference) used for determining size-extensivity corrections.

Table S50. Detailed multiconfigurational results for [$RuCp_2$], $T_1 \rightarrow S_0$ vertical emission energy. [a]

	E (S=0) (a.u.)	E (S=1) (a.u.)	ΔE (eV)
CASSCF(10,12)fix [b]	-478.532390	-478.459370	1.99
CASPT2(10,12)fix [b]	-480.765424	-480.693107	1.97
CASPT2(10,12)fix Frozen 4s4p [b]	-480.379974	-480.304921	2.04
pc-NEVPT2(10,12)fix [b]	-480.739291	-480.659525	2.17
sc-NEVPT2(10,12)fix [b]	-480.729722	-480.650053	2.17
MRCISD(10,12)fix [b]	-480.106404	-480.032857	2.00
MRCISD+Q(D)(10,12)fix [b,c]	-480.566449	-480.492667	2.01
MRCISD+Q(DS)(10,12)fix [b,c]	-480.756438	-480.682512	2.01
MRCISD+Q(P)(10,12)fix [b,c]	-480.718443	-480.644544	2.01
C_0 [d]	0.879675	0.879693	

[a] Single-point calculations performed with the cT(D)-PP basis set, for, for UHF-CCSD(T)/cT(D)-PP geometry of the triplet excited state. [b] "(10,12)fix" means that double-shell orbitals d'xz and d'yz were taken from CASSCF(10,12) state-average calculations of six lowest triplet roots (all components of the T_1, T_2, T_3 states) and not optimized any further. [c] Energies including Davidson (D), Davidson-Silver (DS), or Pople (P) size-extensivity correction (fixed reference). [d] Coefficient of the reference function in the MRCISD wave function (fixed reference) used for determining size-extensivity corrections.

Table S51. Vertical energy difference between S_1 and T_1 excited states of $[FeCp_2]$. [a]

method	basis set	E(T_1) (a.u.)	E(S_1) (a.u.)	ΔE (eV)
CASPT2(10,12)	cT(D)-DK	-1658.346359	-1658.316071	0.82
	cQ-DK [b]	-1658.560073	-1658.530909	0.79
	c5/Q-DK [c]	-1658.580428	-1658.551696	0.78
	estimated CBS limit [d]			0.77
NEVPT2(10,12)	cT(D)-DK	-1658.292827	-1658.266470	0.72
	estimated CBS limit [e]			0.66

[a] Single-point calculations for BP86/def2TZVP geometry of the singlet ground state.
[b] cQ-DK basis set: cc-pwCVQZ-DK (Fe) / cc-pVQZ (C,H).
[c] c5/Q-DK basis set: cc-pwCV5Z-DK (Fe) / cc-pVQZ (C,H).
[d] Estimated from equation $E(CBS) = A + B(X+3/2)^4$, where X=5 for c5/Q-DK, X=4 for cQ-DK.
[e] Estimated as ΔE(NEVPT2/cT(D)-DK) + ΔE(CASPT2/CBS) - ΔE(CASPT2/cT(D)-DK).

Table S52. Vertical energy difference between S_1 and T_1 excited states of $[CoCp_2]^+$. [a]

method	basis set	E(T_1) (a.u.)	E(S_1) (a.u.)	ΔE (eV)
CASPT2(10,12)	cT(D)-DK	-1778.720571	-1778.694292	0.72
	cQ-DK [b]	-1778.936967	-1778.911303	0.70
	c5/Q-DK [b]	-1778.959826	-1778.934579	0.69
	estimated CBS limit [c]			0.68
NEVPT2(10,12)	T(D)-DK	-1778.653838	-1778.629756	0.66
	estimated CBS limit [d]			0.62

[a] Single-point calculations for BP86/def2TZVP geometry of the singlet ground state.
[b] See previous table for definition of cQ-DK and c5/Q-DK basis sets.
[c] Estimated from equation $E(CBS) = A + B(X+3/2)^4$, where X=5 for c5/Q-DK, X=4 for cQ-DK.
[d] Estimated using additive CBS correction taken from CASPT2 calculations, i.e.
ΔE(NEVPT2/CBS) = ΔE(NEVPT2/cT(D)-DK) + ΔE(CASPT2/CBS) - ΔE(CASPT2/cT(D)-DK).

Table S53. Vertical energy difference between S_1 and T_1 excited states of [$RuCp_2$]. [a]

method	basis set	E(T_1) (a.u.)	E(S_1) (a.u.)	ΔE (eV)
CASPT2(10,12)fix	cT(D)-PP	-480.679518	-480.662266	0.47
	cQ-PP [b]	-480.897314	-480.881063	0.44
	c5/Q-PP [c]	-480.919534	-480.903714	0.43
	estimated CBS limit [d]			0.42
NEVPT2(10,12)fix	cT(D)-PP	-480.655757	-480.640728	0.41
	estimated CBS limit [e]			0.36

[a] Single-point calculations for BP86/def2TZVP geometry of the singlet ground state.
[b] cQ-PP basis set: cc-pwCVQZ-PP (Ru) / cc-pVQZ (C, H).
[c] c5/Q-PP basis set cc-pwCV5Z-PP (Ru) / cc-pVQZ (C, H).
[d] Estimated from equation $E(CBS) = A + B(X+3/2)^4$, where X=5 for c5/Q-DK, X=4 for cQ-DK.
[e] Estimated using additive CBS correction taken from CASPT2 calculations, i.e.
ΔE(NEVPT2/CBS) = ΔE(NEVPT2/cT(D)-PP) + ΔE(CASPT2/CBS) - ΔE(CASPT2/cT(D)-PP).

Table S54. Dependence of multiconfigurational results on the choice of active space for [$FeCp_2$], $S_0 \rightarrow T_1$ vertical excitation energy. [a]

method	active space	E (S=0) (a.u.)	E (S=1) (a.u.)	ΔE (eV)
CASSCF	(10,10)	-1656.145101	-1656.055217	2.45
	(10,12)	-1656.152212	-1656.081998	1.91
	(10,12)fix [b]	-1656.151921	-1656.081924	1.90
	(10,14)	-1656.169999	-1656.098149	1.96
	(14,16)	-1656.205764	-1656.118333	2.38
	(18,15)	-1656.156194	-1656.087176	1.88
	(14,18)	-1656.217255	-1656.146197	1.93
CASPT2	(10,10)	-1658.421103	-1658.351072	1.91
	(10,12)	-1658.420670	-1658.346359	2.02
	(10,12)fix [b]	-1658.420595	-1658.346610	2.01
	(10,14)	-1658.420670	-1658.346604	2.02
	(14,16)	-1658.408745	-1658.339415	1.89
	(18,15)	-1658.422995	-1658.357969	1.77
	(14,18)	-1658.409359	-1658.334024	2.05
pc-NEVPT2	(10,10)	-1658.389924	-1658.313551	2.08
	(10,12)	-1658.380034	-1658.292827	2.37
	(10,12)fix [b]	-1658.378917	-1658.293198	2.33
	(10,14)	-1658.388784	-1658.305366	2.27
MRCISD+Q(D) [c]	(10,10)	-1658.222660	-1658.142468	2.18
	(10,12)	-1658.224300	-1658.150229	2.02
	(10,12)fix [b]	-1658.224187	-1658.150299	2.01
	(10,14)	-1658.228896	-1658.154621	2.02

[a] Single point calculations performed for BP86/def2-TZVP structure of the singlet ground state, using the cT(D)-DK basis set. [b] "(10,12)fix" means that double-shell orbitals d'xz and d'yz were taken from CASSCF(10,12) state-average calculations of six lowest triplet roots (all components of the T_1, T_2, T_3 states) and not optimized any further. [c] Energies including Davidson (D) size-extensivity correction (fixed reference).

Table S55. Dependence of multiconfigurational results on the choice of active space for $[CoCp_2]^+$, $S_0 \rightarrow T_1$ vertical excitation energy. [a]

method	active space	E (S=0) (a.u.)	E (S=1) (a.u.)	ΔE (eV)
CASSCF	(10,10)	-1776.529084	-1776.426666	2.79
	(10,12)	-1776.542524	-1776.463180	2.16
	(10,12)fix [b]	-1776.542241	-1776.462885	2.16
CASPT2	(10,10)	-1778.811487	-1778.729047	2.24
	(10,12)	-1778.808319	-1778.720571	2.39
	(10,12)fix [b]	-1778.808326	-1778.720598	2.39
pc-NEVPT2	(10,10)	-1778.762680	-1778.675993	2.36
	(10,12)	-1778.752332	-1778.653838	2.68
	(10,12)fix [b]	-1778.751427	-1778.654010	2.65
MRCISD+Q(D) [c]	(10,10)	-1778.615506	-1778.523846	2.49
	(10,12)	-1778.618071	-1778.532713	2.32
	(10,12)fix [b]	-1778.617977	-1778.532680	2.32

[a] Single-point calculations for BP86/def2-TZVP structure of singlet ground state, using the cT(D)-DK basis set.
[b] "(10,12)fix" means that double-shell orbitals d'xz and d'yz were taken from CASSCF(10,12) state-average calculations of six lowest triplet roots (all components of the T_1, T_2, T_3 states) and not optimized any further.
[c] Energies including Davidson (D) size-extensivity correction (fixed reference).

Table S56. Dependence of multiconfigurational results on the choice of active space for $RuCp_2$, S_0 - T_1 adiabatic energy. [a]

method	active space	E (S=0) (a.u.)	E (S=1) (a.u.)	ΔE (eV)
CASSCF	(10,10)	-478.539548	-478.434462	2.86
	(10,12)fix [b]	-478.541623	-478.449789	2.50
CASPT2	(10,10)	-480.804074	-480.692819	3.03
	(10,12)fix [b]	-480.804256	-480.691941	3.06
pc-NEVPT2	(10,10)	-480.792763	-480.672976	3.26
	(10,12)fix [b]	-480.788554	-480.653236	3.68
MRCISD+Q(D) [c]	(10,10)	-480.591316	-480.481714	2.98
	(10,12)fix [b]	-480.591801	-480.487579	2.84

[a] Single-point calculations for BP86/def2-TZVP structures, using the cT(D)-PP basis set. [b] "(10,12)fix" means that double-shell orbitals d'xz and d'yz were taken from CASSCF(10,12) state-average calculations of six lowest triplet roots (all components of the T_1, T_2, T_3 states) and not optimized any further. [c] Energies including Davidson (D) size-extensivity correction (fixed reference).

Table S57. Dependence of multiconfigurational results on the choice of active space for $RuCp_2$, $S_0 \rightarrow T_1$ vertical excitation energy. [a]

method	active space	E (S=0) (a.u.)	E (S=1) (a.u.)	ΔE (eV)
CASSCF	(10,10)	-478.539548	-478.399368	3.81
	(10,12) [b]	-478.541984	-478.413088	3.51
	(10,12)fix [c]	-478.541623	-478.413041	3.50
CASPT2	(10,10)	-480.804074	-480.679386	3.39
	(10,12) [b]	-480.804375	-480.679426	3.40
	(10,12)fix [c]	-480.804256	-480.679518	3.39
pc-NEVPT2	(10,10)	-480.792763	-480.662643	3.54
	(10,12)fix [c]	-480.788554	-480.655757	3.61
MRCISD+Q(D) [d]	(10,10)	-480.591316	-480.459458	3.59
	(10,12)fix [c]	-480.591801	-480.464195	3.47

[a] Single-point calculations for BP86/def2-TZVP structure of the singlet ground state, with the cT(D)-PP basis set. [b] CASSCF(10,12) for S_0 state could be converged to desired solution only with Molcas. [c] "(10,12)fix" means that double-shell orbitals d'xz and d'yz were taken from CASSCF(10,12) state-average calculations of six lowest triplet roots (all components of the T_1, T_2, T_3 states) and not optimized any further. [d] Energies including Davidson (D) size-extensivity correction (fixed reference).

Table S58. Dependence of multiconfigurational results on the choice of active space for $RuCp_2$, $T_1 \rightarrow S_0$ vertical emission energy. [a]

method	active space	E (S=0) (a.u.)	E (S=1) (a.u.)	ΔE (eV)
CASSCF	(10,10)	-478.529408	-478.446109	2.27
	(10,12)fix [b]	-478.532390	-478.459370	1.99
CASPT2	(10,10)	-480.765536	-480.693761	1.95
	(10,12)fix [b]	-480.765424	-480.693107	1.97
pc-NEVPT2	(10,10)	-480.752107	-480.673660	2.13
	(10,12)fix [b]	-480.739291	-480.659525	2.17
MRCISD+Q(D) [c]	(10,10)	-480.565694	-480.488238	2.11
	(10,12)fix [b]	-480.566449	-480.492667	2.01

[a] Single-point calculations for UHF-CCSD(T)/cT(D)-PP structure of the triplet excited stateperformed, using the T(D)-PP basis set. [b] "(10,12)fix" means that double-shell orbitals d'xz and d'yz were taken from CASSCF(10,12) state-average calculations of six lowest triplet roots (all components of the T_1, T_2, T_3 states) and not optimized any further. [c] Energies including Davidson (D) size-extensivity correction (fixed reference).

Table S59. CASPT2 excitation energies for eclipsed and staggered conformations of $FeCp_2$. [a]

	total energies (a.u.)		excitation energies (eV)	
	eclipsed	staggered [b]	eclipsed	staggered [b]
S_0	-1658.420549	-1658.418280		
T_1	-1658.350187	-1658.350139	1.91	1.85
T_2	-1658.343617	-1658.344104	2.09	2.02
T_3	-1658.331056	-1658.330312	2.44	2.39

[a] All calculations reported at the CASPT2(10,12)/cT(D)-DK level for BP86 geometries. For triplet states SA6 (state-average) calculations were performed. For singlet state, the (10,12)fix approximation was consistently applied for both conformations because fully optimized (10,12) could not be obtained for the staggered one due to undesired orbital rotations. [b] Staggered "conformation" is saddle point at DFT:BP86 level (see main article).

Table S60. Estimated solvation effect (EtOH) on CASPT2 vertical excitation energies for $FeCp_2$. [a]

Spin state	g/g [b]	s/g [c]	g/s [d]	s/s [e]
total energies, in a.u.: [a]				
S_0	-1658.420670	-1658.436072	-1658.420818	-1658.436308
T_1	-1658.350227	-1658.365919	-1658.349369	-1658.365112
T_2	-1658.343723	-1658.359260	-1658.349368	-1658.358311
T_3	-1658.331087	-1658.346869	-1658.342639	-1658.346345
S_1	-1658.318446	-1658.334311	-1658.342647	-1658.333724
S_2	-1658.314502	-1658.330302	-1658.330512	-1658.329377
S_3	-1658.278853	-1658.294622	-1658.330511	-1658.294131
excitation energies from S_0, in eV:				
T_1	1.92	1.91	1.94	1.94
T_2	2.09	2.09	1.94	2.12
T_3	2.44	2.43	2.13	2.45
S_1	2.78	2.77	2.13	2.79
S_2	2.89	2.88	2.46	2.91
S_3	3.86	3.85	2.46	3.87

[a] All energies calculated at CASPT2(10,12)/cT(D)-DK level for BP86 geometries, optimized either in gas phase or within the COSMO model of ethanol (ε=24.3); excitation energies calculated either in gas phase or within the PCM model (ethanol) with non-equilibrium solvation of excited states. [b] g/g = Geometry optimized and vertical excitations energy calculated in gas phase. [c] s/g = Energy calculation in solvent model for geometry optimized in gas phase. [d] g/s = Energies calculated in gas phase for geometry optimized in solvent model. [e] s/s = Energies calculated in solvent model for geometry optimized in solvent model.

Table S61. Estimated solvation effect (water) on CASPT2 vertical exc. energies for $[CoCp_2]^+$. [a]

Spin state	g/g [b]	s/g [c]	g/s [d]	s/s [e]
total energies, in a.u.: [a]				
S_0	-1778.808319	-1778.899297	-1778.808783	-1778.900123
T_1	-1778.724819	-1778.817094	-1778.723410	-1778.816026
T_2	-1778.721705	-1778.814059	-1778.720231	-1778.812884
T_3	-1778.700855	-1778.793169	-1778.699811	-1778.792430
S_1	-1778.696549	-1778.788659	-1778.694940	-1778.786966
S_2	-1778.696148	-1778.788395	-1778.695093	-1778.787607
S_3	-1778.658096	-1778.750179	-1778.657013	-1778.749412
excitation energies from S_0, in eV:				
T_1	2.27	2.24	2.32	2.29
T_2	2.36	2.32	2.41	2.37
T_3	2.92	2.89	2.97	2.93
S_1	3.04	3.01	3.10	3.08
S_2	3.05	3.02	3.09	3.06
S_3	4.09	4.06	4.13	4.10

[a] All energies calculated at CASPT2(10,12)/cT(D)-DK level for BP86 geometries, optimized either in gas phase or within the COSMO model of water (ε=80.4); excitation energies calculated either in gas phase or within the PCM model (water) with non-equilibrium solvation of excited states. [b] g/g = Geometry optimized and vertical excitations energy calculated in gas phase. [c] s/g = Energy calculation in solvent model for geometry optimized in gas phase. [d] g/s = Energies calculated in gas phase for geometry optimized in solvent model. [e] s/s = Energies calculated in solvent model for geometry optimized in solvent model.

Table S62. Estimate solvation effect (heptane) on CASPT2 vertical excitation energies for $RuCp_2$. [a]

Spin state	g/g [b]	s/g [c]	g/s [d]	s/s [e]
total energies, in a.u.: [a]				
S_0	-4914.464025	-4914.469705	-4914.463948	-4914.469475
T_1	-4914.342643	-4914.347789	-4914.342830	-4914.347985
T_2	-4914.335122	-4914.340241	-4914.335256	-4914.340469
T_3	-4914.328365	-4914.333464	-4914.328544	-4914.333652
S_1	-4914.325680	-4914.331005	-4914.325835	-4914.331170
S_2	-4914.318740	-4914.324127	-4914.319026	-4914.324356
S_3	-4914.299345	-4914.304588	-4914.299512	-4914.304765
excitation energies from S_0, in eV:				
T_1	3.30	3.32	3.30	3.31
T_2	3.51	3.52	3.50	3.51
T_3	3.69	3.71	3.68	3.70
S_1	3.76	3.77	3.76	3.76
S_2	3.95	3.96	3.94	3.95
S_3	4.48	4.49	4.47	4.48

[a] All energies calculated at CASPT2(10,12)/cT(D)-DK level for BP86 geometries, optimized either in gas phase or within the COSMO model of heptane (ε=1.92); excitation energies calculated either in gas phase or within the PCM model (heptane) with non-equilibrium solvation of excited states. [b] g/g = Geometry optimized and vertical excitations energy calculated in gas phase. [c] s/g = Energy calculation in solvent model for geometry optimized in gas phase. [d] g/s = Energies calculated in gas phase for geometry optimized in solvent model. [e] s/s = Energies calculated in solvent model for geometry optimized in solvent model.

Table S63. Estimated solvation effect (EtOH) on CASPT2 vertical excitation energies for $RuCp_2$. [a]

Spin state	g/g [b]	s/g [c]	g/s [d]	s/s [e]
total energies, in a.u.: [a]				
S_0	-4914.464025	-4914.481378	-4914.463573	-4914.481061
T_1	-4914.342643	-4914.358135	-4914.343069	-4914.358637
T_2	-4914.335122	-4914.350675	-4914.335514	-4914.351263
T_3	-4914.328365	-4914.343904	-4914.328777	-4914.344368
S_1	-4914.325680	-4914.341547	-4914.326029	-4914.341976
S_2	-4914.318740	-4914.334595	-4914.319294	-4914.335136
S_3	-4914.299345	-4914.315180	-4914.299727	-4914.315643
excitation energies from S_0, in eV:				
T_1	3.30	3.35	3.28	3.33
T_2	3.51	3.56	3.48	3.53
T_3	3.69	3.74	3.67	3.72
S_1	3.76	3.81	3.74	3.78
S_2	3.95	3.99	3.93	3.97
S_3	4.48	4.52	4.46	4.50

[a] All energies calculated at CASPT2(10,12)/cT(D)-DK level for BP86 geometries, optimized either in gas phase or within the COSMO model of ethanol (ε=24.55); excitation energies calculated either in gas phase or within the PCM model (ethanol) with non-equilibrium solvation of excited states. [b] g/g = Geometry optimized and vertical excitations energy calculated in gas phase. [c] s/g = Energy calculation in solvent model for geometry optimized in gas phase. [d] g/s = Energies calculated in gas phase for geometry optimized in solvent model. [e] s/s = Energies calculated in solvent model for geometry optimized in solvent model.

Table S64. Estimate of spin-orbit coupling (SOC) effect on CASPT2 vertical excitation energies for $RuCp_2$, ground state equilibrium geometry (S_0). [a]

spin state [b]	Total energies (a.u.)		Relative energies (eV)		
	without SOC	with SOC	without SOC	with SOC	with SOC avg [c]
S_0	-4914.465545	-4914.466094	0.00	0.00	0.00
		-4914.341244		3.40	
T_1	-4914.338346	-4914.338535	3.46	3.47	3.46
		-4914.336982		3.51	
		-4914.332222		3.64	
T_2	-4914.330417	-4914.332018	3.68	3.65	3.68
		-4914.328816		3.74	
		-4914.324800		3.84	
T_3	-4914.324093	-4914.324321	3.85	3.86	3.88
		-4914.321577		3.93	
S_1	-4914.321782	-4914.321481	3.91	3.94	3.94
S_2	-4914.314461	-4914.312656	4.11	4.18	4.18
S_3	-4914.295363	-4914.295247	4.63	4.65	4.65

[a] The SOC was included within the AMFI approximation, based on CASSCF(10,12) wave functions and CASPT2(10,12) energies, cT(D)-DK basis set, based on PBE0 geometry of S_0. The S_0 (SS) and S_1,S_2,S_3 (SA6) and T_1,T_2,T_3 (SA6) data were supplied to the RASSI program and allowed to interact through the SOC Hamiltonian. Calculations were performed with the C_s symmetry. [b] Dominant parentage for SOC states. [c] Average energy of SOC levels with common (dominant) parentage.

Table S65. Estate of spin-orbit coupling (SOC) effect on CASPT2 vertical energies of singlet and triplet states for RuCp2, lowest triplet state (T_1) equilibrium geometry. [a]

spin state [b,c]	Total energies (a.u.)		Relative energies (eV)		
	without SOC	with SOC	without SOC	with SOC	with SOC avg [d]
1 ^{1}A' (S_0)	-4914.424436	-4914.425319	0.00	0.00	0.00
		-4914.357106		1.86	
1 ^{3}A" (T_1)	-4914.355650	-4914.356992	1.87	1.86	1.87
		-4914.356111		1.88	
		-4914.348429		2.09	
2 ^{3}A"	-4914.347507	-4914.346741	2.09	2.14	2.13
		-4914.346291		2.15	
		-4914.342209		2.26	
3 ^{3}A"	-4914.341388	-4914.341637	2.26	2.28	2.27
		-4914.341560		2.28	
		-4914.338300		2.37	
4 ^{3}A"	-4914.336534	-4914.337176	2.39	2.40	2.39
		-4914.337010		2.40	
1 ^{1}A"	-4914.335390	-4914.334363	2.42	2.48	2.48
		-4914.329041		2.62	
5 ^{3}A"	-4914.327839	-4914.326666	2.63	2.68	2.66
		-4914.326623		2.69	
2 ^{1}A"	-4914.326245	-4914.324633	2.67	2.74	2.74
3 ^{1}A"	-4914.323463	-4914.322325	2.75	2.80	2.80
		-4914.321173		2.83	
6 ^{3}A"	-4914.321478	-4914.321070	2.80	2.84	2.84
		-4914.321037		2.84	
4 ^{1}A"	-4914.316144	-4914.315403	2.95	2.99	2.99
5 ^{1}A"	-4914.299330	-4914.299112	3.40	3.43	3.43
6 ^{1}A"	-4914.296056	-4914.295924	3.49	3.52	3.52

[a] The SOC was included within the AMFI approximation, based on CASSCF(10,12) wave functions and CASPT2(10,12) energies, cT(D)-DK basis set, based on PBE0 geometry of T_1. The S_0 (SS) and S_1,S_2,S_3 (SA6) and T_1,T_2,T_3 (SA6) data were supplied to the RASSI program and allowed to interact through the SOC Hamiltonian. Calculations were performed under the C_s symmetry. [b] Dominant parentage for SOC states. [c] Using irreps of C_s (computational symmetry group); only S_0 and T_1 states are explicitly identified. [c] Average energy of SOC levels with common (dominant) parentage.

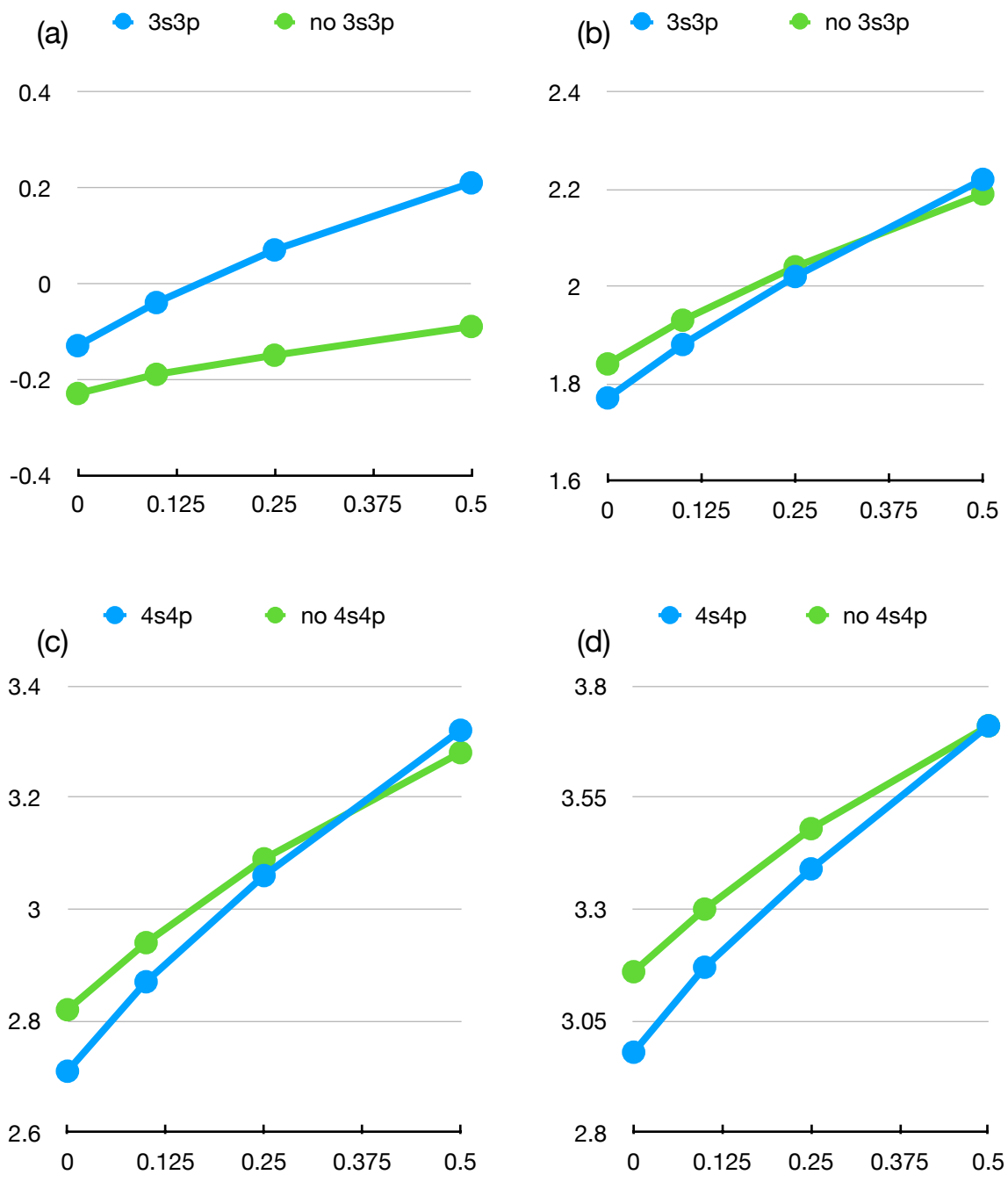

Figure S10: Dependence of CASPT2 relative energies (values in eV) on the IPEA shift parameter (values in au) for (a) ^{2,6}[MnCp2] (adiabatic energy), (b) ^{1,3}[FeCp2] (vertical excitation energy), (c) ^{1,3}[RuCp2] (adiabatic energy), (d) ^{1,3}[RuCp2] (vertical excitation energy) with the outer-core electrons (3s3p/4s4p) being either correlated or frozen at the CASPT2 level. Results were obtained from CASPT2(10,12)/cT(D)-DK (a, b) or CASPT2(10,12)fix/cT(D)-PP calculations.

8. Multireference character

Table S66. Diagnostics of multireference character

Diagnostics	Spin state [a]	$MnCp_2$	$RuCp_2$			$FeCp_2$	$[CoCp_2]^+$
		(adiab) [f,i]	(adiab) [g,j]	(vert abs) [g,j]	(vert emi) [h,j]	(vert abs) [g,i]	(vert abs) [g,i]
T_1 [b]	lower	0.035	0.021	0.021	0.024	0.044	0.043
	higher	0.015	0.030	0.028	0.021	0.036	0.033
D_1 [b]	lower	0.148	0.081	0.081	0.102	0.193	0.183
	higher	0.058	0.163	0.167	0.091	0.186	0.166
T_1^{KS} [b,c]	lower	0.009	0.009	0.009	0.009	0.009	0.009
	higher	0.013	0.010	0.012	0.010	0.009	0.011
D_1^{KS} [b,c]	lower	0.021	0.023	0.023	0.025	0.021	0.024
	higher	0.049	0.027	0.056	0.024	0.021	0.047
C_0^2 [d]	lower	0.891	0.922	0.922	0.914	0.868	0.862
	higher	0.986	0.924	0.827	0.929	0.830	0.877
M [e]	lower	0.074	0.039	0.039	0.047	0.073	0.099
	higher	0.014	0.052	0.257	0.051	0.199	0.139

[a] Lower spin state is the one with smaller value of *S* i.e. doublet for $MnCp_2$, singlet for others; higher spin state - the one with larger value of *S*, i.e., sextet for $MnCp_2$, triplet for others. [b] At UCCSD/cT(D)-DK level. [c] Using KS orbitals. [d] Weight of leading configuration in CASSCF(10,12) (state specific). [e] From occupation numbers of CASSCF(10,12) natural orbitals (state specific). [f] PBE0/def2TZVP geometry. [g] BP86/def2TZVP geometries, *h* UHF-CCSD(T) geometry. [i] cT(D)-DK basis set. [j] cT(D)-PP basis set.

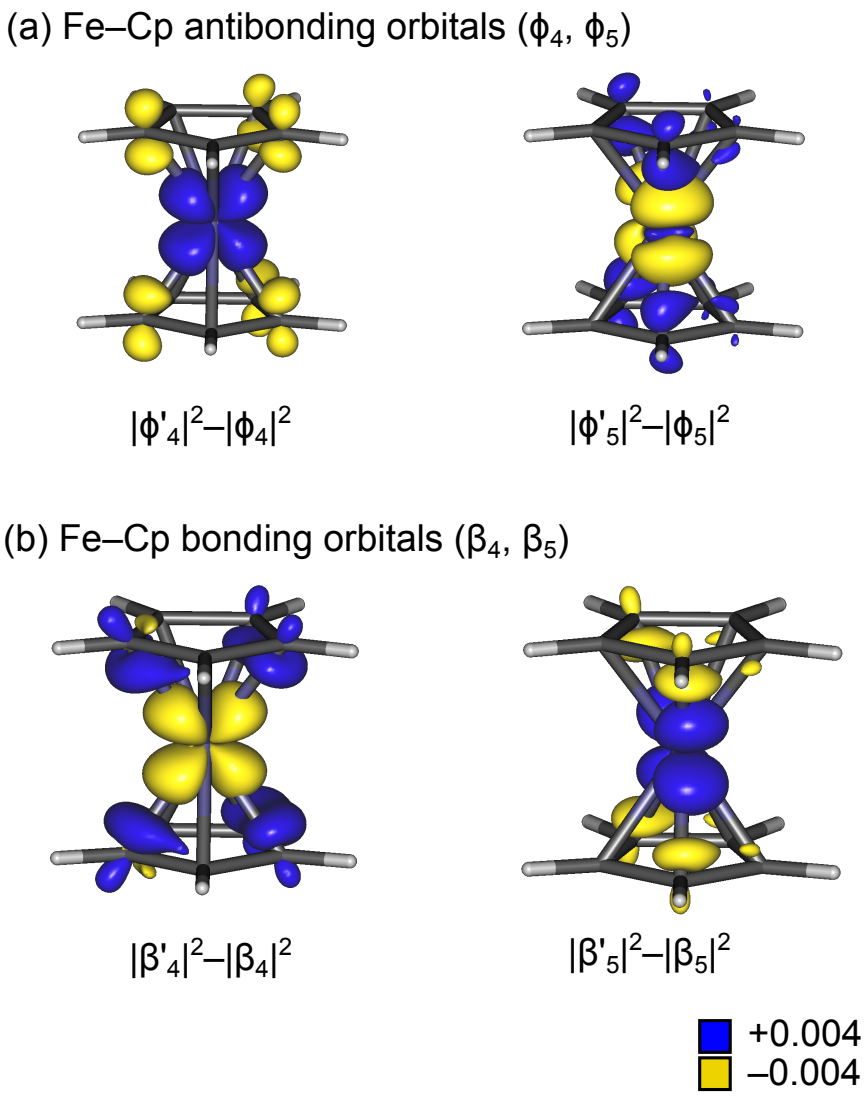

Figure S11. Contour plots of differences between SS and SA2(avg) orbitals for the T_1 state (computed vertically for S_0 geometry, BP86) of $FeCp_2$ from CASSCF(10,12): (a) for orbitals ϕ_4 (singly occupied) and ϕ_5 (unoccupied) having antibonding character; (b) for corresponding bonding orbitals β_4 and β_5. The quantity plotted is the difference between the squared module of an orbital from SS (with prime) and of the corresponding orbital from SA2 calculations (without prime).

9. Experimental spectrum of ferrocene

Extended baseline correction: the baselines of different measurements were adjusted to minimize the sum of squared deviations between the ε values obtained from different reliable measurements for the same wavelength, i.e.

$$\sum_{\lambda}\sum_{i\neq j}\left(\frac{A_i^{\lambda}-s_i}{c_i l_i}-\frac{A_j^{\lambda}-s_j}{c_j l_j}\right)^2 a_{ij}^{\lambda}=\min$$

where A_i^{λ} is the absorbance at wavelength λ obtained from the *i*-th measurement; c_i and l_i are the molar concentration and the cuvette path length for the *i*-th measurement; s_i is the unknown baseline shift for the *i*-th measurement (to be found); factor a_{ij}^{λ} serves to exclude unreliable measurements (a_{ij}^{λ} = 1 if both A_i^{λ} and A_j^{λ} fall in range 0.05 to 2; a_{ij}^{λ} = 0 otherwise). This is a typical least-squares problem, which leads to the linear system of equations for the vector of unknowns s_i

$$\boldsymbol{M}\boldsymbol{s}=\boldsymbol{b},$$

with matrices ***M*** and ***b*** defined as

$$M_{ij}=\sum_{\lambda}\left(-\delta_{ij}\sum_{k\neq i}a_{ik}^{\lambda}+(1-\delta_{ij})a_{ij}^{\lambda}\right)\frac{1}{c_i c_j l_i l_j}$$

$$b_i=\sum_{\lambda}\sum_{k\neq i}\left(\frac{A_k^{\lambda}}{c_k l_k}-\frac{A_i^{\lambda}}{c_i l_i}\right)\frac{a_{ik}^{\lambda}}{c_i l_i}$$

(δ_{ij} is the Kronecker delta). This linear system is underdetermined with one free parameter. We choose this parameter to minimize the norm of the **s** vector, i.e. to find the set of smallest possible baseline shifts which satisfy the least-squares problem.

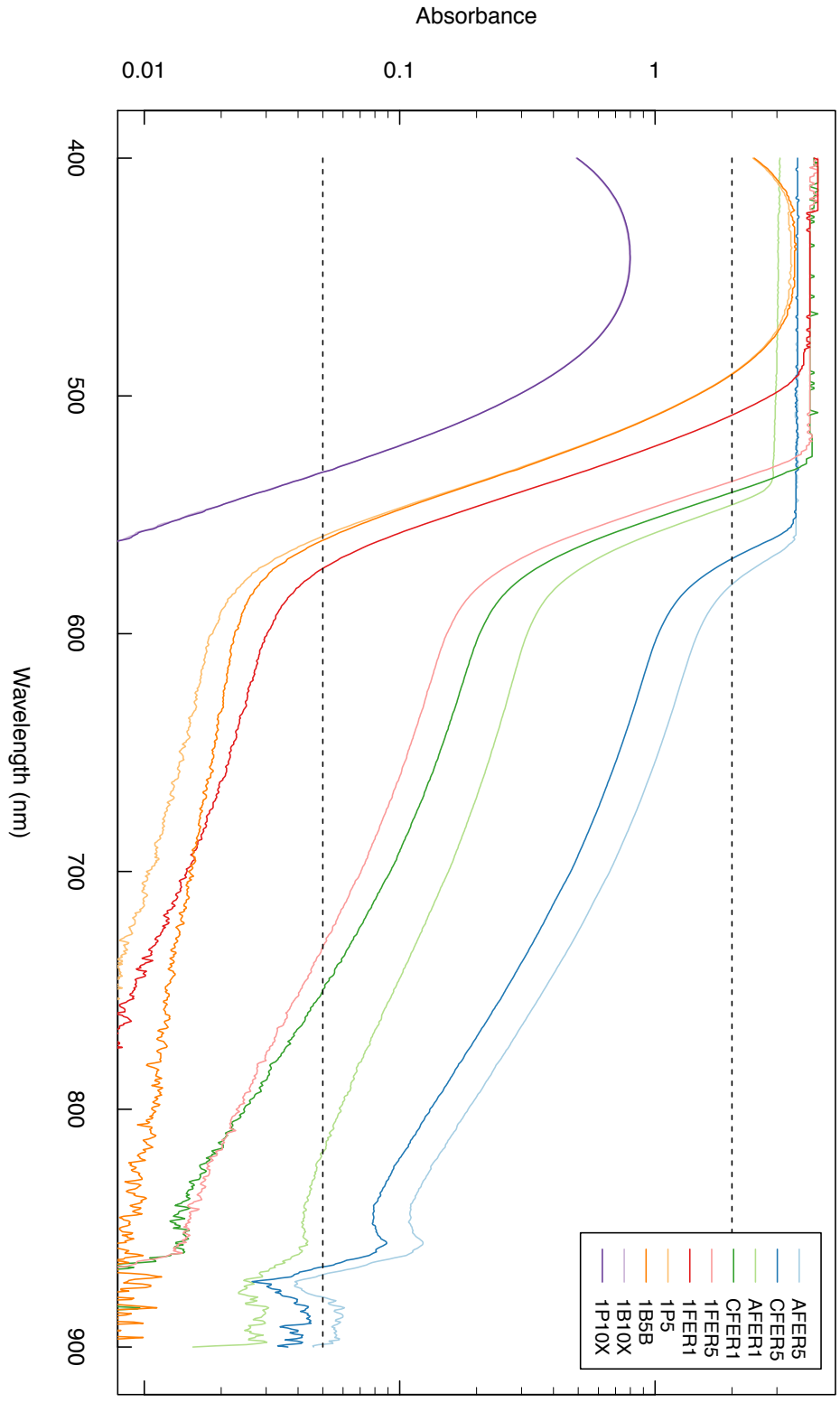

Figure S12. Absorbance spectra of ferrocene in benzene acquired for different concentrations and cuvette lengths (reported as "lab code": molar concentration *c*, cuvette length): AFER5: 0.8029M, 5cm; AFER1: same *c*, 1cm; CFER5: 0.5595M, 5cm; CFER1: same *c*, 1cm; 1FER5: 0.08136M, 5cm; 1FER1: same *c*, 1cm; 1P5 and 1B5B: 0.008136M, 5cm; 1B10X and 1P10X: same *c*, 1cm. Dashed lines define reliable absorbance window 0.05 to 2.

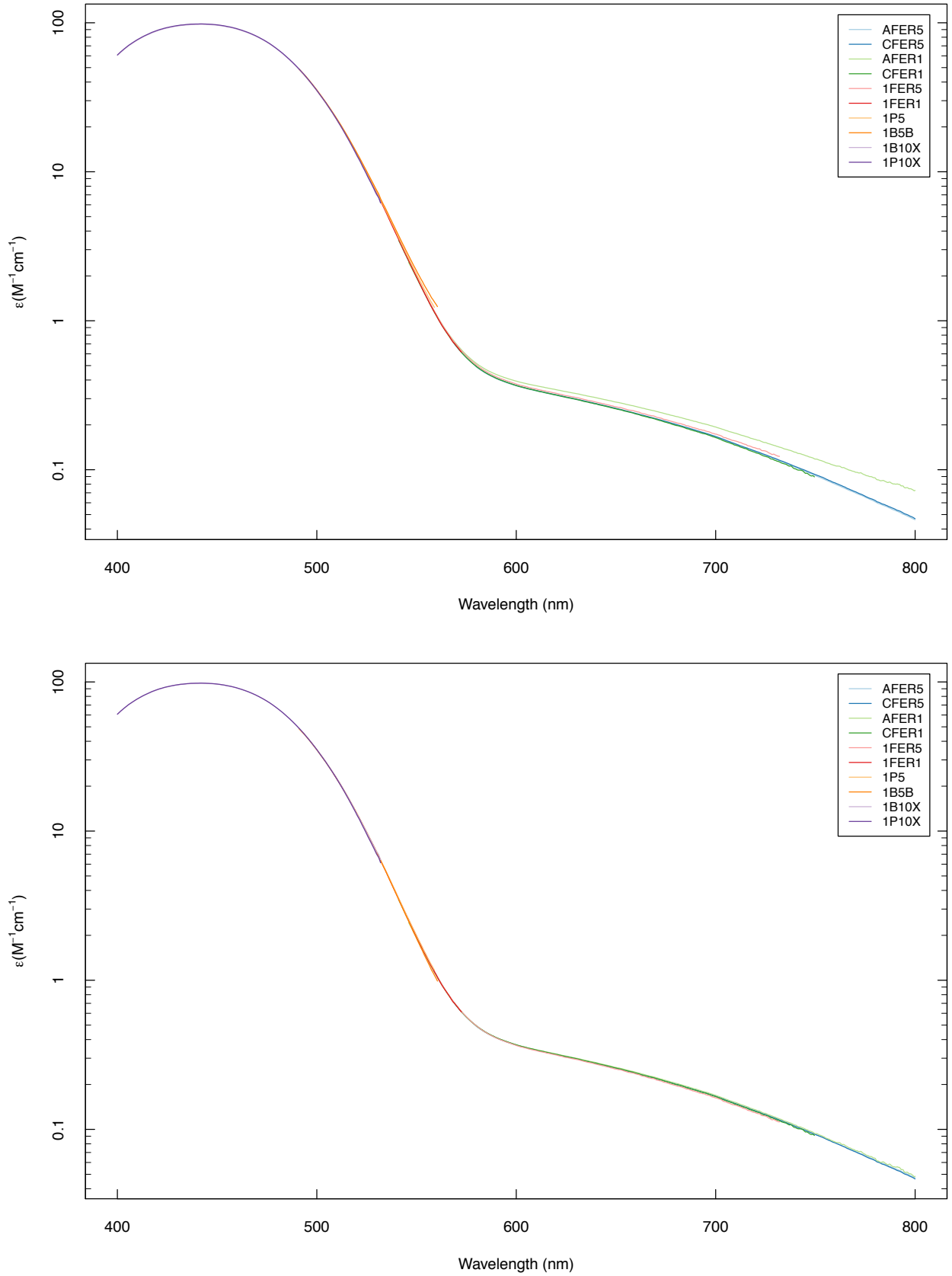

Figure S13. Overlapped extinction coefficient spectra from different measurements in the wavelength range 400-800 nm (excluding unreliable absorbances with $A < 0.05$ or $A > 2$). The spectral baselines are before the extended baseline correction (*top*) or after (*bottom*). See previous figure for description of experimental conditions corresponding to given "lab codes".

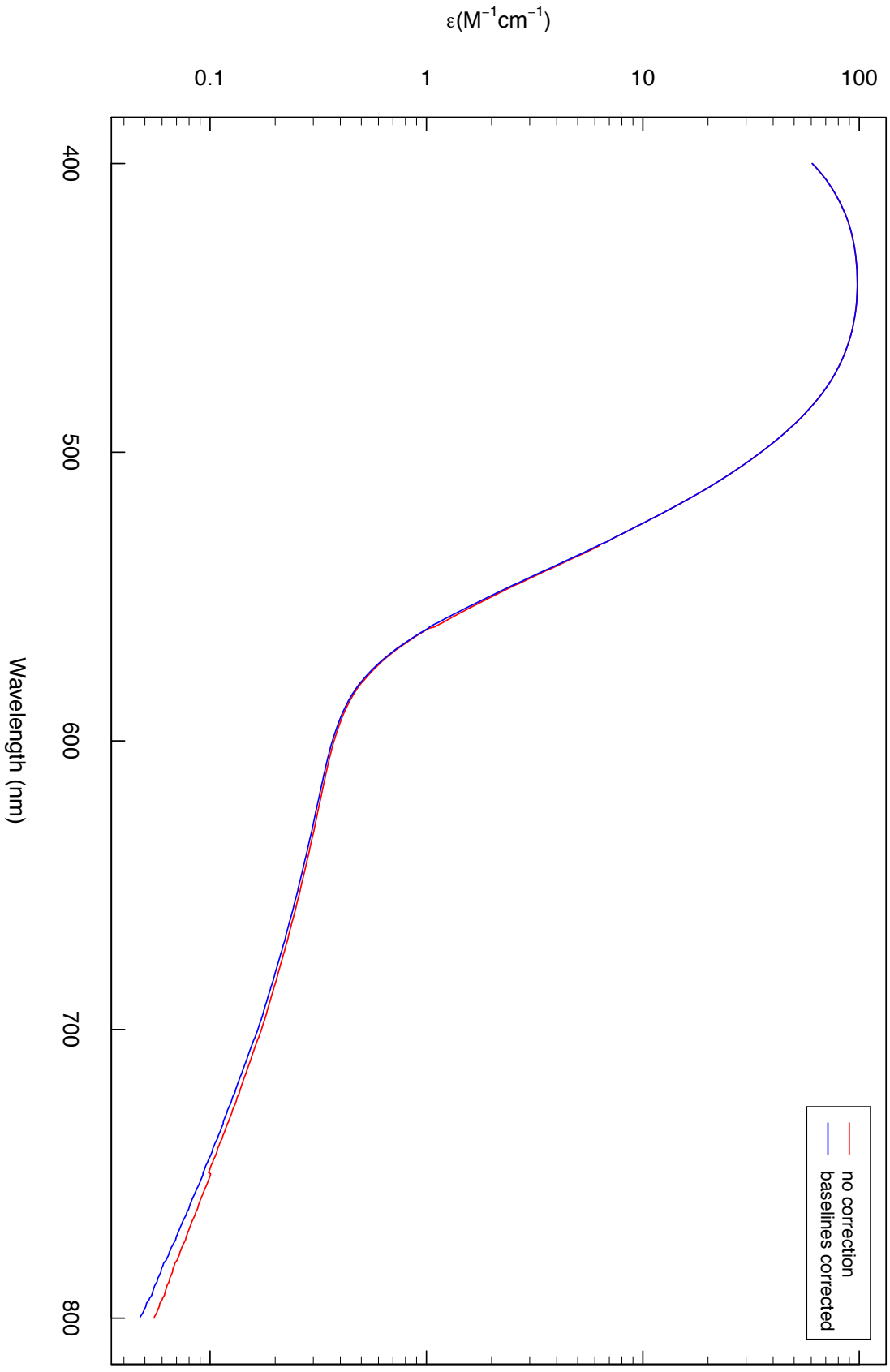

Figure S14. Averaged molar extinction coefficient spectrum of ferrocene in benzene obtained without (*red*) and with (*blue*) the extended baseline correction.

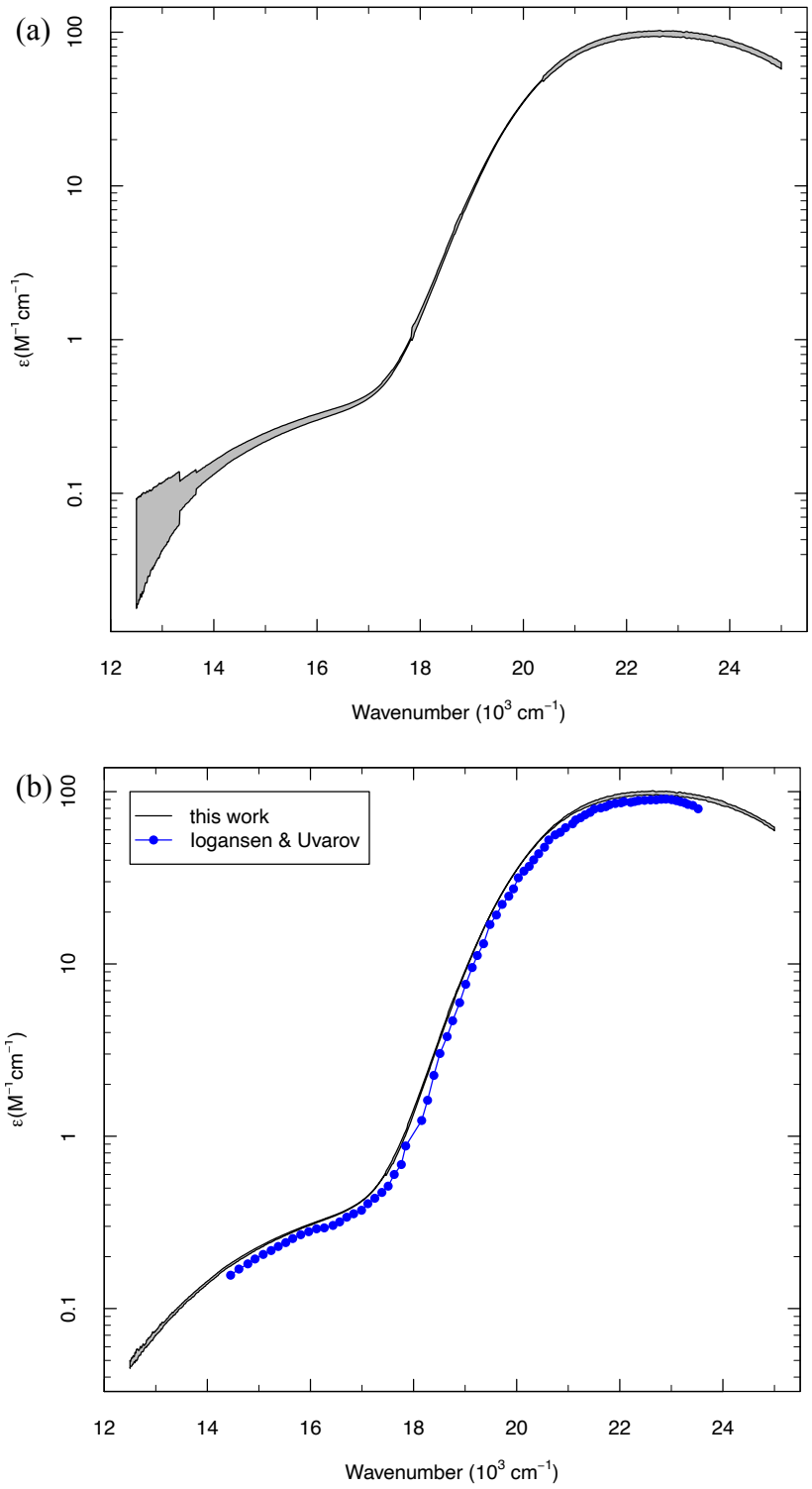

Figure S15. Averaged molar extinction coefficient spectrum of ferrocene in benzene with error estimation (shaded area is 95%-confidence interval) obtained without (a) or with (b) extended baseline correction. Figure (b) additionally contains the spectrum of ferrocene in ethanol digitalized from the paper by Iogansen and Uvarov (ref 29*)

*In ref. 29 the spectrum is split in two parts using different scales (ε 0-100 for range 400-550 nm, and ε 0-0.9 for range 560-700 nm). When presenting these data in Figure S15, the last two points of the first range were removed because they have huge relative errors (as corresponding to almost zero intensity in the appropriate scale). In fact, if these points were retained, there would appear an unphysical bump in the spectrum presented as a single plot in the log scale.

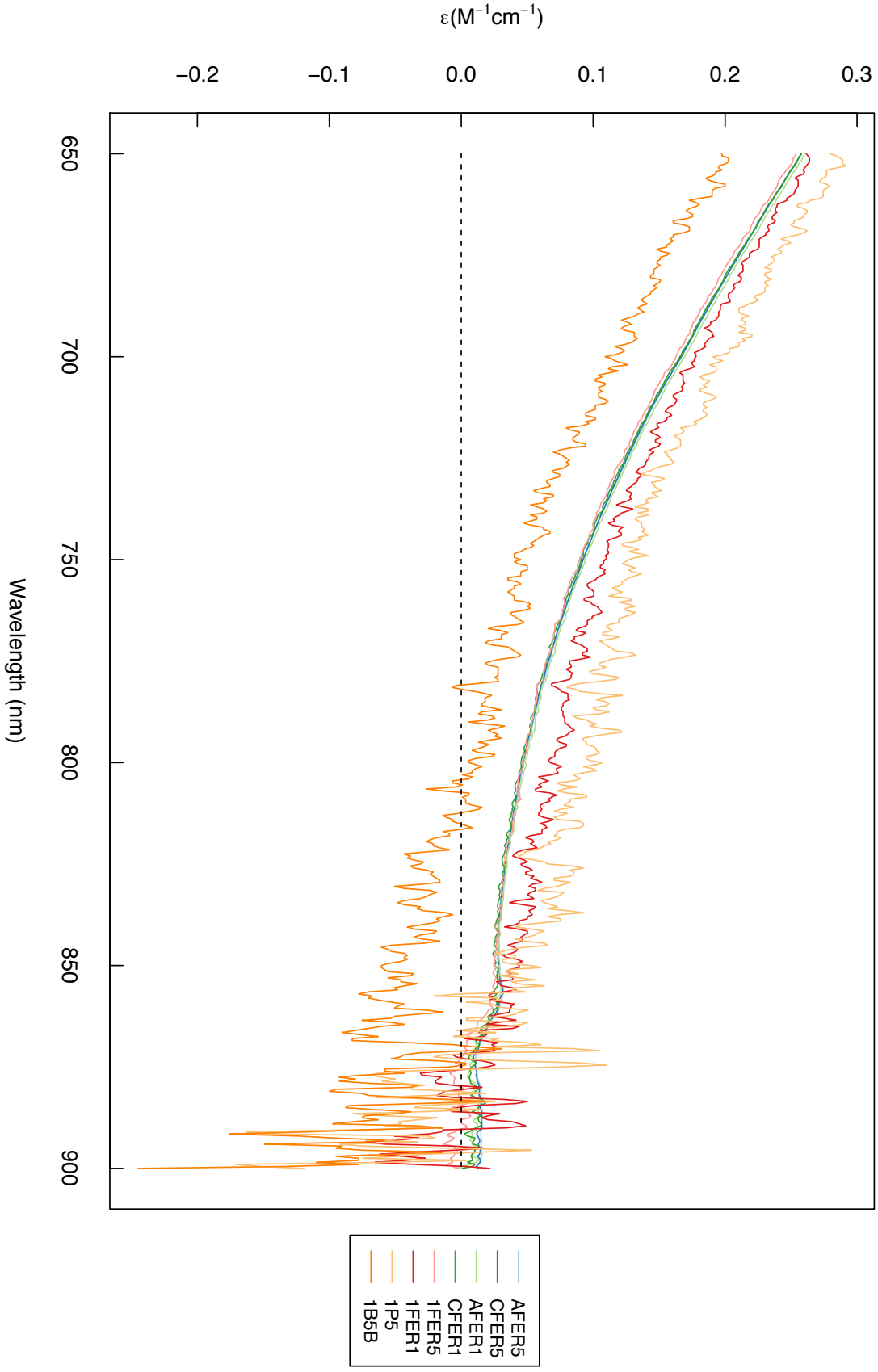

Figure S16. Absorbance tails in the low-energy region of ferrocene in benzene which is dominated by spectral noise. Note that the only data used by us to prepare the averaged spectrum were 1FER5 up to 732 nm, CFER1 up to 749.5 nm, and AFER5, AFER1, CFER5 up to 800 nm. All other (noisy) data or any data above 800 nm are not interpreted by us.

10. Additional references

10.1 Basis sets

def2-TZVP, def2-TZVPP, def2-QZVPP
[S1] F. Weigend, M. Häser, H. Patzelt and R. Ahlrichs *Chem. Phys. Lett.*, 1998, **294**, 143-152.
[S2] F. Weigend, F. Furche, R. Ahlrichs, *J. Chem. Phys.*, 2003, **119**, 12753-12762
[S3] F. Weigend, R. Ahlrichs, *Phys. Chem. Chem. Phys.*, 2005, **7**, 3297-3305.

STO TZ2P, TZ2P+
[S4] E. Van Lenthe and E. J. Baerends, *J. Comp. Chem.*, 2003, **24**, 1142-1156

cc-pwCVTZ, cc-pwCVnZ-DK (n=T, Q, 5) for Mn, Fe, Co
[S5] N.B. Balabanov and K.A. Peterson, *J. Chem. Phys.*, 2006, **125**, 074110.

cc-pwCVnZ-PP (n=T, Q, 5) for Ru
[S6] K.A. Peterson, D. Figgen, M. Dolg, M. and H. Stoll, *J. Chem. Phys.*, 2007, **126**, 124101

cc-pVTZ, cc-pVDZ
[S7] T.H. Dunning, *J. Chem. Phys.*, 1989, **90**, 1007-1023.

cc-pVnZ-DK (n=D, T, Q)
[S8] W.A. de Jong, R.J. Harrison, and D.A. Dixon, *J. Chem. Phys.*, 2001, **114**, 48-53.

aug-cc-pVTZ/mp2fit for Fe
[S9] J. G. Hill and J. A. Platts, *J. Chem. Phys.*, 2008, **128**, 044104.

aug-cc-pVTZ/mpf2fit for main-group elements
[S10] F. Weigend, A. Köhn, C. Hättig, *J. Chem. Phys.*, 2002, **116**, 3175-3183.

def2-TZVPP/jkfit for Fe
[S11] F. Weigend, *J. Comp. Chem.* 2008, **29**, 167-175

aug-cc-pVTZ/jkfit for main-group elements
[S12] F. Weigend, *Phys. Chem. Chem. Phys.* 2002, **4**, 4285-4291.

aug-cc-pVTZ/optri for main-group elements
[S13] K.E. Yousaf and K.A. Peterson, *Chem. Phys. Lett.* 2009, **476**, 303-307.

aug-cc-pVTZ-PP/mp2fit for Ru
[S14] J.G. Hill and J.A. Platts, *J. Chem. Theory Comput.* 2009, **5**, 500-505.

10.2 Density functionals

PBE

[S15] J. P. Perdew, K. Burke and M. Ernzerhof, *Phys. Rev. Lett.*, 1996, **77**, 3865–3868.

BLYP

[S16] A. D. Becke, *Phys. Rev. A.*, 1988, **38**, 3098–3100.
[S17] (a) C. Lee, W. Yang and R. G. Parr, *Phys. Rev. B*, 1988, **37**, 785–789; (b) B. Miehlich, A. Savin, H. Stoll and H. Preuss, *Chem. Phys. Lett.,* 1989, **157**, 200–206.

OLYP, OPBE

[S18] N. C. Handy and A. J. Cohen, *Mol. Phys.,* 2001, 99, 403–412.

OPBE

[S19] M. Swart, A. R. Groenhof, A. W. Ehlers and K. Lammerstsma, *J. Phys. Chem. A*, 2004, 108, 5479–5483.

B97D

[S20] S. Grimme, *J. Comput. Chem.*, 2006, 27, 1787–1799.

TPSS

[S21] J. Tao, J. P. Perdew, V. N. Staroverov and G. E. Scuseria, *Phys. Rev. Lett.*, 2003, 91, 146401.

M06, M06L

[S22] Y. Zhao and D. G. Truhlar, *Theor. Chem. Acc*., 2008, 120, 215–241.

MN15L

[S23] H. S. Yu, X. He and D. G. Truhlar, *J. Chem. Theory Comput.*, 2016, 12, 1280–1293.

MVS, MVSh

[S24] J. Sun, J. P. Perdew and A. Ruzsinszky, *Proc. Natl. Acad. Sci. U. S. A*., 2015, 112, 685–689.

BR89

[S25] A. D. Becke and M. R. Roussel, *Phys. Rev. A: At., Mol., Opt. Phys*., 1989, 39, 3761–3767.

PBE0

[S26] J. P. Perdew, M. Ernzerhof and K. Burke, *J. Chem. Phys.*, 1996, 105, 9982–9985.

B3LYP

[S27] (a) A. D. Becke, *J. Chem. Phys.*, 1993, 98, 5648–5652; (b) P. J. Stephens, F. J. Devlin, C. F. Chabalowski and M. J. Frisch, *J. Phys. Chem*., 1994, 98, 11623–11627.

TPSSh

[S28] J. P. Perdew, J. Tao, V. N. Staroverov and G. E. Scuseria, *J. Chem. Phys*., 2004, 120, 6898–6911.

PW6B95

[S29] Y. Zhao and D. G. Truhlar, *J. Phys. Chem. A*, 2005, 109, 5656–5667.

MN15
[S30] H. S. Yu, X. He, S. L. Li and D. G. Truhlar, *Chem. Sci.*, 2016, 7, 5032–5051.

LC-wPBE
[S31] T. M. Henderson, A. F. Izmaylov, G. Scalmani and G. E. Scuseria, *J. Chem. Phys*., 2009, 131, 044108.

CAM-B3LYP
[S32] T. Yanai, D. P. Tew and N. C. Handy, *Chem. Phys. Lett.*, 2004, 393, 51–57.

wB97XD
[S33] J.-D. Chai and M. Head-Gordon, *Phys. Chem. Chem. Phys.*, 2008, 10, 6615–6620.

LC-BLYP
[S34] H. Iikura, T. Tsuneda, T. Yanai and K. Hirao, *J. Chem. Phys*., 2001, 115, 3540–3544.

M11
[S35] R. Peverati and D. G. Truhlar, *J. Phys. Chem. Lett.*, 2011, 2, 2810–2817.

M11L
[S36] R. Peverati and D. G. Truhlar, *J. Phys. Chem. Lett*., 2012, 3, 117–124.

LH14t-calPBE
[S37] A. V. Arbuznikov and M. Kaupp, *J. Chem. Phys.*, 2014, 141, 204101.

B2PLYP
[S38] S. Grimme, *J. Chem. Phys.,* 2006, 124, 034108.

S12g, S12h
[S39] M. Swart, *Chem. Phys. Lett*., 2013, 580, 166–171.

B3LYP*
[S40] M. Reiher, O. Salomon and B. A. Hess, *Theor. Chem. Acc*., 2001, 107, 48–55.

10.3 Computational packages (complete references from main article)

[55] CFOUR, a quantum chemical program package written by J.F. Stanton, J. Gauss, L. Cheng, M.E. Harding, D.A. Matthews, P.G. Szalay with contributions from A.A. Auer, R.J. Bartlett, U. Benedikt, C. Berger, D.E. Bernholdt, Y.J. Bomble, O. Christiansen, F. Engel, R. Faber, M. Heckert, O. Heun, M. Hilgenberg, C. Huber, T.-C. Jagau, D. Jonsson, J. Jusélius, T. Kirsch, K. Klein, W.J. Lauderdale, F. Lipparini, T. Metzroth, L.A. Mück, D.P. O'Neill, D.R. Price, E. Prochnow, C. Puzzarini, K. Ruud, F. Schiffmann, W. Schwalbach, C. Simmons, S. Stopkowicz, A. Tajti, J. Vázquez, F. Wang, J.D. Watts and the integral packages MOLECULE (J. Almlöf and P.R. Taylor), PROPS (P.R. Taylor), ABACUS (T. Helgaker, H.J. Aa. Jensen, P. Jørgensen, and J. Olsen), and ECP routines by A. V. Mitin and C. van Wüllen. For the current version, see http://www.cfour.de.

[56] E. J. Baerends, T. Ziegler, A. J. Atkins, J. Autschbach, D. Bashford, O. Baseggio, A. Bérces, F. M. Bickelhaupt, C. Bo, P. M. Boerritger, L. Cavallo, C. Daul, D. P. Chong, D. V. Chulhai, L. Deng, R. M. Dickson, J. M. Dieterich, D. E. Ellis, M. van Faassen, A. Ghysels, A. Giammona, S. J. A. van Gisbergen, A. Goez, A. W. Götz, S. Gusarov, F. E. Harris, P. van den Hoek, Z. Hu, C. R. Jacob, H. Jacobsen, L. Jensen, L. Joubert, J. W. Kaminski, G. van Kessel, C. König, F. Kootstra, A. Kovalenko, M. Krykunov, E. van Lenthe, D. A. McCormack, A. Michalak, M. Mitoraj, S. M. Morton, J. Neugebauer, V. P. Nicu, L. Noodleman, V. P. Osinga, S. Patchkovskii, M. Pavanello, C. A. Peeples, P. H. T. Philipsen, D. Post, C. C. Pye, H. Ramanantoanina, P. Ramos, W. Ravenek, J. I. Rodríguez, P. Ros, R. Rüger, P. R. T. Schipper, D. Schlüns, H. van Schoot, G. Schreckenbach, J. S. Seldenthuis, M. Seth, J. G. Snijders, M. Solà, S. M., M. Swart, D. Swerhone, G. te Velde, V. Tognetti, P. Vernooijs, L. Versluis, L. Visscher, O. Visser, F. Wang, T. A. Wesolowski, E. M. van Wezenbeek, G. Wiesenekker, S. K. Wolff, T. K. Woo and A. L. Yakovlev, *ADF2017*, SCM, Theoretical Chemistry, Vrije Universiteit, Amsterdam, The Netherlands, https://www.scm.com.

[57] M. J. Frisch, G. W. Trucks, H. B. Schlegel, G. E. Scuseria, M. A. Robb, J. R. Cheeseman, G. Scalmani, V. Barone, G. A. Petersson, H. Nakatsuji, X. Li, M. Caricato, A. V. Marenich, J. Bloino, B. G. Janesko, R. Gom- perts, B. Mennucci, H. P. Hratchian, J. V. Ortiz, A. F. Izmaylov, J. L. Sonnenberg, D. Williams-Young, F. Ding, F. Lipparini, F. Egidi, J. Goings, B. Peng, A. Petrone, T. Henderson, D. Ranasinghe, V. G. Zakrzewski, J. Gao, N. Rega, G. Zheng, W. Liang, M. Hada, M. Ehara, K. Toyota, R. Fukuda, J. Hasegawa, M. Ishida, T. Nakajima, Y. Honda, O. Kitao, H. Nakai, T. Vreven, K. Throssell, J. A. Montgomery, Jr., J. E. Peralta, F. Ogliaro, M. J. Bearpark, J. J. Heyd, E. N. Brothers, K. N. Kudin, V. N. Staroverov, T. A. Keith, R. Kobayashi, J. Normand, K. Raghavachari, A. P. Rendell, J. C. Burant, S. S. Iyengar, J. Tomasi, M. Cossi, J. M. Millam, M. Klene, C. Adamo, R. Cammi, J. W. Ochterski, R. L. Martin, K. Morokuma, O. Farkas, J. B. Foresman and D. J. Fox, *Gaussian 16 Revision B.01*, 2016, Gaussian Inc. Wallingford CT.

[61] H.-J. Werner, P. J. Knowles, G. Knizia, F. R. Manby, M. Schütz, P. Celani, W. Györffy, D. Kats, T. Korona, R. Lindh, A. Mitrushenkov, G. Rauhut, K. R. Shamasundar, T. B. Adler, R. D. Amos, A. Bernhardsson, A. Berning, D. L. Cooper, M. J. O. Deegan, A. J. Dobbyn, F. Eckert, E. Goll, C. Hampel, A. Hesselmann, G. Hetzer, T. Hrenar, G. Jansen, C. Köppl, Y. Liu, A. W. Lloyd, R. A. Mata, A. J. May, S. J. McNicholas, W. Meyer, M. E. Mura, A. Nicklass, D. P. O'Neill, P. Palmieri, D. Peng, K. Pflüger, R. Pitzer, M. Reiher, T. Shiozaki, H. Stoll, A. J. Stone, R. Tarroni, T. Thorsteinsson and M. Wang, MOLPRO, version 2015, a package of ab initio programs, see http://www.molpro.net.

[63] Aquilante, F.; Autschbach, J.; Baiardi, A.; Battaglia, S.; Borin, V. A.; Chibotaru, L. F.; Conti, I.; De Vico, L.; Delcey, M.; Fdez. Galván, I.; Ferré, N.; Freitag, L.; Garavelli, M.; Gong, X.; Knecht, S.; Larsson, E. D.; Lindh, R.; Lundberg, M.; Malmqvist, P. Å.; Nenov, A.; Norell, J.; Odelius, M.; Olivucci, M.; Pedersen, T. B.; Pedraza-González, L.; Phung, Q. M.; Pierloot, K.; Reiher, M.; Schapiro, I.; Segarra-Martí, J.; Segatta, F.; Seijo, L.; Sen, S.; Sergentu, D.-C.; Stein, C. J.; Ungur, L.; Vacher, M.; Valentini, A. & Veryazov, V. "Modern quantum chemistry with [Open]Molcas"
J. Chem. Phys., 2020, **152**, 214117.